JEM Article

Local changes in lipid environment of TCR microclusters regulate membrane binding by the CD3 ϵ cytoplasmic domain

Etienne Gagnon,^{1,3} David A. Schubert,¹ Susana Gordo,¹ H. Hamlet Chu,¹ and Kai W. Wucherpfennig^{1,2}

The CD3 ϵ and ζ cytoplasmic domains of the T cell receptor bind to the inner leaflet of the plasma membrane (PM), and a previous nuclear magnetic resonance structure showed that both tyrosines of the CD3 ϵ immunoreceptor tyrosine-based activation motif partition into the bilayer. Electrostatic interactions between acidic phospholipids and clusters of basic CD3 ϵ residues were previously shown to be essential for CD3 ϵ and ζ membrane binding. Phosphatidylserine (PS) is the most abundant negatively charged lipid on the inner leaflet of the PM and makes a major contribution to membrane binding by the CD3 ϵ cytoplasmic domain. Here, we show that TCR triggering by peptide–MHC complexes induces dissociation of the CD3 ϵ cytoplasmic domain from the plasma membrane. Release of the CD3 ϵ cytoplasmic domain from the membrane is accompanied by a substantial focal reduction in negative charge and available PS in TCR microclusters. These changes in the lipid composition of TCR microclusters even occur when TCR signaling is blocked with a Src kinase inhibitor. Local changes in the lipid composition of TCR microclusters thus render the CD3 ϵ cytoplasmic domain accessible during early stages of T cell activation.

CORRESPONDENCE
Kai Wucherpfennig:
kai_wucherpfennig@
dfci.harvard.edu
OR
Etienne Gagnon:
etienne.gagnon@umontreal.ca

Abbreviations used: APB, antigenpresenting bead; cSMAC, central supramolecular activation cluster; DAG, diacylglycerol; FLIM, fluorescence lifetime imaging microscopy; FRAP, fluorescence recovery after photobleaching; FRET, Forster resonance energy transfer; ITAM, immunoreceptor tyrosine-based activation motif; mRFP, monomeric RFP; NMR, nuclear magnetic resonance; PIP2, phosphatidylinositol 4,5-bisphosphate; pMHC, peptide-MHC; PS, phosphatidylserine; TCSPC, time-correlated singlephoton counting; TIRFM, total internal reflection fluorescence microscopy.

TCR signaling controls many different aspects of T cell function. The ligand-binding TCR heterodimer assembles with three dimeric signaling modules (CD3 $\gamma\varepsilon$, CD3 $\delta\varepsilon$, and $\zeta\zeta$) that contain cytoplasmic immunoreceptor tyrosinebased activation motifs (ITAMs), characterized by two tyrosines and two aliphatic residues (YxxL/I₆₋₁₂YxxL/I; Reth, 1989; Kuhns et al., 2006). After phosphorylation of both ITAM tyrosines by the Src kinase Lck, ZAP-70 is bound through its tandem SH2 domains. Engagement of both ZAP-70 SH2 domains destabilizes its inactive state, and ZAP-70 then phosphorylates downstream substrates, including LAT and SLP-76, which function as scaffolds for recruitment of many signaling molecules (Balagopalan et al., 2010; Jordan and Koretzky, 2010; Wang et al., 2010).

TCR recognition is highly sensitive: transient calcium flux can be induced by one or a few peptide–MHC (pMHC) ligands at the interface between T cells and APCs, and \sim 10 ligands are sufficient for sustained calcium flux

(Irvine et al., 2002). Several mechanisms prevent ligand-independent TCR activation, including phosphatases that can dephosphorylate TCR ITAMs or downstream signaling molecules (Kuhns et al., 2006). After recognition of agonist pMHC ligands, TCRs form microclusters that physically exclude the phosphatases CD45 and CD148, which have substantially larger extracellular domains than the TCR (Choudhuri et al., 2005; Varma et al., 2006). Interestingly, TCR microclusters even form when the most proximal kinase in the cascade, Lck, is pharmacologically inhibited with PP2 (Campi et al., 2005). TCR binding to pMHC molecules occurs with rapid kinetics, due to the alignment of the interacting molecules on opposing membranes. Off-rates are very fast (typical $t_{1/2}$ of less than one second), and productive signaling

Downloaded from http://rupress.org/jem/article-pdf/209/13/2423/1744139/jem_20120790.pdf by guest on 02 December 2025

¹Department of Cancer Immunology and AIDS, Dana-Farber Cancer Institute; and ²Program in Immunology, Harvard Medical School, Boston, MA 02115

³Département de Microbiologie et Immunologie, Institut de Recherche en Immunologie et Cancer, Montréal, Quebec, H3T 1J4, Canada

^{© 2012} Gagnon et al. This article is distributed under the terms of an Attribution-Noncommercial-Share Alike-No Mirror Sites license for the first six months after the publication date (see http://lwww.rupress.org/terms). After six months it available under a Creative Commons License (Attribution-Noncommercial-Share Alike 3.0 Unported license, as described at http://creativecommons.org/licenses/by-nc-sa/3.0/).

in microclusters results from many sequential binding events (serial triggering; Valitutti et al., 1995; Huang et al., 2010; Huppa et al., 2010).

Studies by several groups have shown that the cytoplasmic domains of the CD3 ε and ζ chains are not suspended in the cytosol, but rather bound to the inner leaflet of the plasma membrane (PM). Membrane binding of CD3 ε and ζ cytoplasmic domains is primarily mediated by clusters of basic residues that interact with anionic lipids, including phosphatidylserine (PS) and phosphatidylinositol species (such as phosphatidylinositol 4,5-bisphosphate; PIP2; Aivazian and Stern, 2000; Sigalov et al., 2006; Xu et al., 2008; DeFord-Watts et al., 2009, 2011; Zhang et al., 2011). Structural studies of the CD3ε cytoplasmic domain in a lipid-bound state by nuclear magnetic resonance (NMR) spectroscopy showed that the two tyrosines of the ITAM can partition into the hydrophobic core of the lipid bilayer (Xu et al., 2008). The NMR data also indicated that this binding mode is dynamic, and a shift in the equilibrium of lipid-bound versus unbound state may thus render the tyrosines accessible during TCR triggering. In vitro studies showed that lipid binding can prevent phosphorylation of the ITAM tyrosine residues by recombinant Lck (Xu et al., 2008).

Here, we investigated mechanisms responsible for dissociation of the CD3 ϵ cytoplasmic domain from the plasma membrane during TCR signaling. We identified early local changes in the lipid composition of TCR microclusters that reduced the density of PS as well as the negative charge of the inner leaflet of the PM. This was accompanied by a decrease in lateral diffusion of PS in the immunological synapse. These results identify a mechanism for release of the CD3 ϵ cytoplasmic domain from the PM during T cell activation.

RESULTS

Membrane binding by the CD3 ϵ cytoplasmic domain in human T cells

We previously reported a Forster resonance energy transfer (FRET)—based approach for imaging membrane binding by the CD3 ϵ cytoplasmic domain (CD3 ϵ _{CD}) in live cells. A fluorescent reporter protein (monomeric teal fluorescent protein 1; TFP) was attached to the CD3 ϵ C terminus (FRET donor) and high FRET values were measured in Jurkat cells when the membrane was labeled with R18, a lipophilic rhodamine derivative (FRET acceptor). These experiments demonstrated close proximity between the CD3 ϵ C terminus and the PM (Xu et al., 2008). Membrane binding by the ζ chain has also been visualized with this technique (Zhang et al., 2011). Assembly of TCR and CD3 chains is quite inefficient, and the cytoplasmic domain of CD3 ϵ was therefore fused to the extracellular/TM domains of a protein that is efficiently transported to the PM (KIR2DL3).

In the current study, we examined whether CD3 $\epsilon_{\rm CD}$ binds to the PM in T cells when the CD3 ϵ chain is incorporated into a full TCR–CD3 complex. Phosphorylation of the CD3 ζ cytoplasmic domain was shown to interfere with rebinding to the PM (Aivazian and Stern, 2000). A CD3 ϵ protein that

is phosphorylated upon TCR triggering would thus not be a useful probe for testing the binding properties of the PM after T cell activation. We generated a human CD3ε construct in which the two ITAM tyrosines were mutated to phenylalanine (a conservative substitution that only removes the hydroxyl groups of the tyrosine residues). TFP was attached to the CD3 $\varepsilon_{\rm CD}$ C terminus for FRET measurements, and an epitope tag (HA) was added to the N terminus for monitoring surface expression (CD3ε-YF-TFP). This construct was introduced into a human T cell clone (B-A8) that recognizes the influenza hemagglutinin 306-318 peptide (HA₃₀₆₋₃₁₈) bound to HLA-DR4 (DRA, DRB1*04:01; abbreviated as HA-DR4). Transduced T cells expressed both the introduced mutant CD3ε chain, as well as the endogenous WT CD3 ε chain, and were found to express normal levels of CD3 ε , as well as other relevant receptors on the cell surface (Fig. 1 B). We also assessed formation of immunological synapses using a lipid bilayer system (Grakoui et al., 1999) with mobile HA-DR4 complexes and ICAM-1. T cells expressing the CD3ε-YF-TFP chain formed normal synapses, and TCR microclusters were readily visualized based on TFP fluorescence (Fig. 1 A). Confocal microscopy and FACS analysis demonstrated surface expression of the CD3ε-YF-TFP chain, but a CD3ε WT protein with a C-terminal TFP group was largely retained in intracellular compartments (Fig. 1, C and D). This phenotype may be caused by more rapid internalization of a TFP-tagged CD3 ε chain, possibly due to basal phosphorylation observed for this protein (unpublished data).

We previously used a steady-state FRET approach to examine membrane binding by CD3 $\varepsilon_{\rm CD}$ (Xu et al., 2008). However, it is difficult to use this approach to quantify $CD3\varepsilon_{CD}$ dissociation during T cell activation because TCR clustering greatly increases local TFP fluorescence, whereas energy transfer reduces the fluorescence of individual TFP molecules. A solution to this problem is to measure FRET by fluorescence lifetime imaging microscopy (FLIM). The fluorescence lifetime is a sensitive indicator of FRET and is independent of donor density, meaning that no corrections for TCR clustering are necessary (Sun et al., 2011b). FLIM data acquisition is performed by repeated low intensity excitation of the fluorophore with a pulsed laser, and the emitted photons are captured and cumulated per pixel in a time-correlated fashion to generate fluorescence decay curves. Time-correlated single-photon counting (TCSPC) allows fitting of the fluorescence decay curve with single, double, or triple exponential decay algorithms, depending on the type of fluorophore or FRET state. A major advantage of FLIM-based approaches is that FRET measurements can be performed with high spatial resolution on a pixel-by-pixel basis.

We first performed FLIM measurements of CD3ε-YF-TFP molecules on nonactivated T cells. FLIM data were obtained by continuously scanning TFP-expressing cells for 40 s using a multiphoton pulsed sapphire laser (820 nm wavelength, 6% power), and little to no photo-bleaching was observed using these settings. TCSPC data were used to generate color-coded images of fluorescence lifetimes (Fig. 2 A).

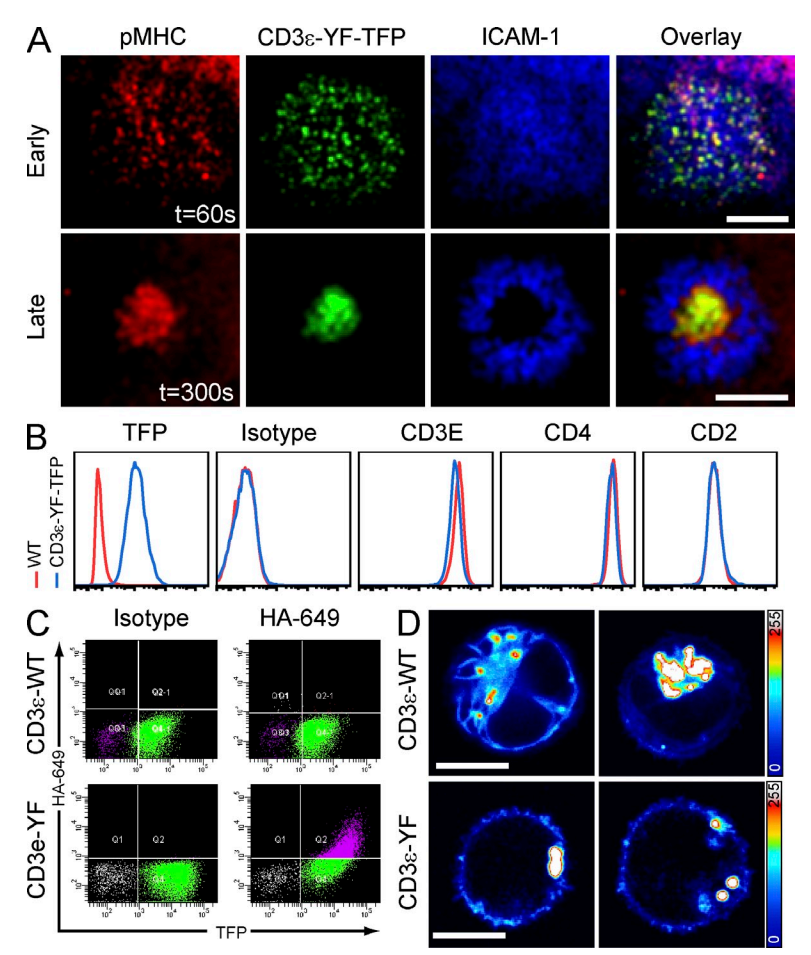


Figure 1. Expression of a CD3ε FRET probe in a human T cell clone. HA-tagged CD3ε chain was expressed through lentiviral infection in human T cell clone B-A8 specific for the influenza ${\rm HA_{306-318}}$ peptide. The two ITAM tyrosines were mutated to phenylalanine (YF). TFP was added to the C terminus for FRET measurements (CD3ε-YF-TFP). Data are representative of n > 3 experiments. (A) T cells expressing CD3 ϵ -YF-TFP were applied on lipid bilayers displaying HA-DR4 and ICAM-1. Synapse formation was imaged by TRIFM at 30-s intervals; shown are representative examples of synapses at early (60 s) and later (300 s) time points. Bars, 10 μm . (B) FACS analysis of CD3 ϵ and TFP expression, representative of three separate experiments. (C) B-A8 T cells expressing CD3ε WT or YF mutant were stained with HA epitope tag or isotype control antibody (Dylight649 labeled) to measure surface expression of CD3 ε constructs. (D) Localization of CD3 ε WT or YF mutant protein was determined by confocal microscopy; pseudocolor gradient indicates signal intensity. Bars, 10 μm.

TFP yielded a single exponential decay curve with a mean fluorescence lifetime of 2,546 picoseconds (ps; \pm 95 ps) at the PM (Fig. 2, B–D). These data are consistent with previously published FLIM values for this fluorescent protein (Padilla-Parra et al., 2009). It is worth noting that the TFP fluorescence lifetime was shorter in intracellular vesicles, possibly due to an acidic environment or degradation. These internal structures serve as a control given that the TFP lifetime should not change when R 18 is incorporated into the PM (Fig. 2 A).

When R18 was injected into the flow cell, the fluorescence lifetime of TFP decreased markedly because of FRET between TFP and R18. The presence of FRET was validated by analysis of fluorescence decay curves. Population analyses using single exponential decay curve fitting of steady-state FLIM or FRET-FLIM showed an overall decrease in TFP fluorescence lifetime of \sim 20% (to 2,034 \pm 230 ps; Fig. 2, B–D and F). When fluorescence decay curves were fitted using dual exponential decay with a fixed long-lived component set at 2,550 ps (the fluorescence lifetime of TFP in the absence of FRET), we were able to identify a FRET component with a lifetime of 1,350–1,600 ps (Fig. 2, E and F). Dual exponential decay calculations improved curve fitting, seen in a decrease of the χ^2 values (Fig. 2 F, in red). This short-lived

component represented 35–55% of all donor molecules at the PM (Fig. 2 F). These results indicate that 35–55% of TFP molecules are in close proximity to the R18 acceptor, with an average FRET efficiency of 43%. These results are in agreement with our previous FRET results with the steady-state approach (FRET values of ~45% with donor quenching approach, ~38% with donor dequenching approach; Xu et al., 2008), even though the human T cells were not as brightly labeled by R18 as previously used Jurkat cells. To our knowledge, this is the first time that FLIM has been used to study dynamic membrane binding by a cytoplasmic domain in live cells.

Dissociation of the CD3& cytoplasmic domain from the membrane during peptide-MHC engagement

We next used this system to address one of our central questions: does the local membrane environment of TCR microclusters change during T cell activation? We first aimed to compare T cell membrane inside and outside of synapses from the same confocal sections. We generated glass-supported lipid bilayers on silica beads displaying mobile HA-DR4 and ICAM-1 (antigen-presenting beads; APB). T cells were allowed to interact with the beads for 60 s, and the flow cell was then

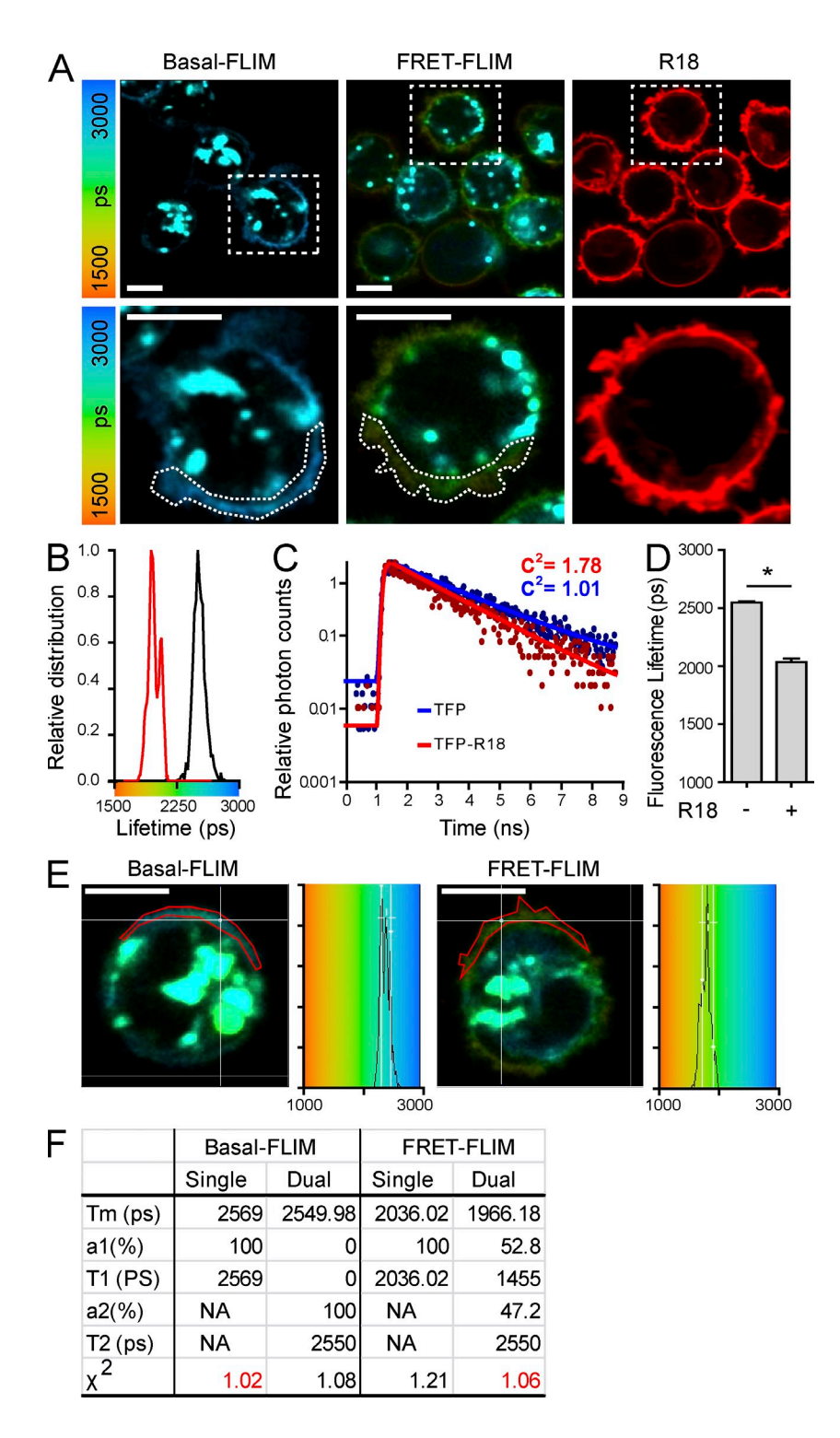


Figure 2. Membrane binding by the CD3 ϵ cytoplasmic domain in primary human T cells. B-A8 T cells expressing CD3ε-YF-TFP were placed into a flow cell and prepared for FLIM acquisition. All data are representative of n > 3 experiments. (A) Membrane binding by CD3 ε_{CD} by FLIM in nonstimulated T cells. FLIM images of TFP (FRET donor) were taken before (basal FLIM) and after injection of R18 (FRET acceptor, 1 μg/ml, 90 s; FRET-FLIM). TCSPC counting was performed and processed using SPCImage. Fluorescence decay was calculated, and color-coded images were generated (color coding range, 1,000-3,000 ps). Shown are basal FLIM of TFP (left), FRET-FLIM after PM was labeled with R18 (middle), and R18 labeling of cells (right). Internal vesicles showed no differences in FLIM during R18 incorporation into the PM. Bars, 10 μm. (B) Relative distribution of mean fluorescence TFP lifetime per pixel at the PM ± R18 (basal FLIM, black line; FRET-FLIM, red line). (C) TFP fluorescence decay curves at PM in presence (red) or absence of R18 (blue). Single pixel TCSPC measurements were fitted to fluorescence decay curves using single exponential decay in SPCImage, minimizing χ^2 values. Increases in slope and χ^2 values indicate presence of multiple fluorophore states due to FRET. (D) TFP population analysis shows 20% decrease of overall fluorescence lifetime in presence of FRET acceptor; error bars represent SEM. n > 10 cells per experiment. (E) Examples of basal-FLIM and FRET-FLIM colorcoded images taken from SPCImage software during analysis. Pictures show color-coded gradient of TFP fluorescent lifetime. Red ROI was used to generate graphs of relative distribution of fluorescence lifetime of photons. White crosshair indicates pixels that were used to generate fluorescence decay curves. Bars, 10 μm. (F) Fluorescence decay curves were calculated from single pixels, highlighted by white cross-hair in E, using either single or dual exponential decay algorithms, optimizing for low χ^2 values. Dual exponential decay calculations were made using a fixed long-lived component, set at 2,550 ps, based on mean TFP fluorescence lifetime in absence of R18 for a population of 30 cells (D). Mean fluorescence lifetimes (Tm), as well as short- and long-lived fluorescent lifetime components (T1 and T2, respectively), are presented. Also, relative abundance of short- and long-lived components (a1 and a2, respectively) is shown. Best fit for data are represented, and lowest χ^2 values are highlighted in red. For basal FLIM measurements, a single exponential decay function yielded an optimal χ^2 value (1.02), whereas a dual exponential decay function was optimal for FRET-FLIM (χ^2 of 1.06).

rapidly washed with cold PBS to capture this early stage of T cell activation. Cells were subsequently labeled with R18 in cold PBS and FLIM data were acquired, all of which was performed within 5 min of bead–cell interactions. Cells that formed an IS with the APB accumulated fluorescent CD3 ϵ at the contact site and typically showed some remodeling of the PM to accommodate the shape of the beads (Fig. 3 A).

The results showed a substantial reduction in FRET efficiency at the synapse (Fig. 3, B and D). The fluorescence lifetime was longer at the synapse (2,397 \pm 90 ps) compared with noncontact areas (2,140 \pm 124 ps), indicating that a substantial fraction of CD3 $\epsilon_{\rm CD}$ was no longer associated with the PM (Fig. 3, B–E and G). Differences in fluorescence decay inside or outside of synapses were observable

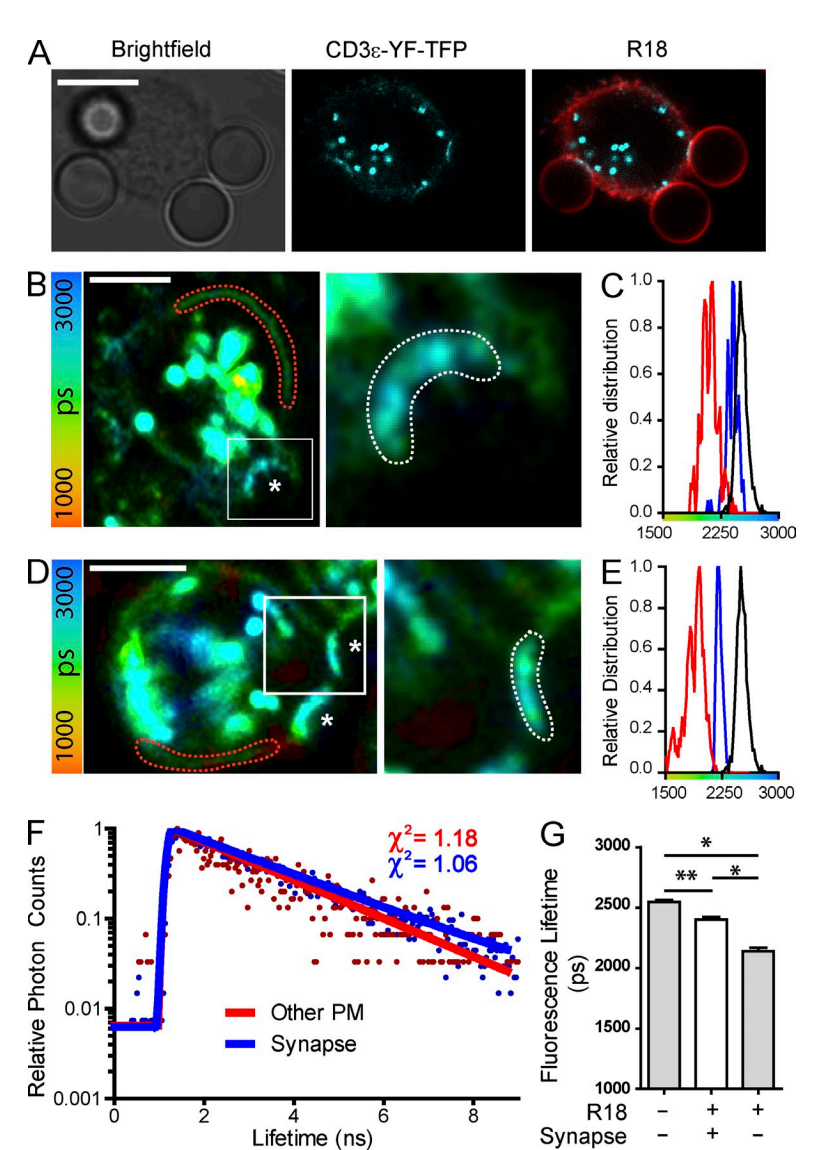


Figure 3. Dissociation of the CD3ε cytoplasmic domain from the plasma membrane after TCR stimulation with peptide-MHC. T cells expressing the CD3_€-YF-TFP probe were stimulated with HA-DR4/ICAM-1 lipid beads. Shortly after bead engagement, cells were labeled with R18 in cold PBS and imaged to acquire FLIM data. Beads forming synapses are indicated (*). All data are representative of n > 3 experiments. (A) Confocal image of CD3ε-YF-TFP-expressing T cells forming synapses with HA-DR4/ICAM-1 lipid beads. Local accumulation of CD3ε is observed at bead-cell interface. Bar, 10 μm. (B and D) Cells with significant accumulation of CD3 ε -YF-TFP probe at synapse and uniform R18 labeling were used for quantification. Right panel shows zoomed area of inset. FLIM measurements were taken at synapse and nonsynapse membrane (ROI delineated by white and red dotted lines, respectively). Bar, 10 µm. (C and E) Relative distribution of mean TFP fluorescence lifetime per pixel during FLIM-FRET within and outside synapse (blue and red line, respectively), compared with basal FLIM (black line). (F) TFP fluorescence decay curves at synapse (blue) and outside synapse (red, other PM). (G) Population analysis of FLIM measurements inside or outside of synapse (syn), compared with basal FLIM before R18 labeling; error bars represent SEM. P-values were calculated using an unpaired two-tailed Student's t test with a 99% CI (*, > 0.0001; **, 0.152). n > 5-10 cells per experiment and condition.

using single exponential decay algorithms (Fig. 3 F). Dual exponential algorithms did not significantly improve curve fitting for the synapse region, indicating that a dominant short-lived fluorophore population was not present (not depicted). There was a moderate reduction in the fluorescence lifetime measured at the synapse in the presence of R18 $(2,397 \pm 90 \text{ ps}; P < 0.001)$ compared with the basal lifetime in the absence of R18 (2,546 \pm 95 ps; Fig. 3 G), possibly because not all TCR-CD3 complexes within the synapse area participated in pMHC recognition/signaling. These results demonstrate that the CD3ε cytoplasmic domain dissociates from the PM at the immunological synapse during activation of human T cells with a pMHC ligand. These results also suggest that phosphorylation of the ITAMs is not a prerequisite for membrane dissociation because the two ITAM tyrosines had been mutated to phenylalanine in this reporter.

Reduced density of anionic lipids on the inner leaflet of the PM during early stages of TCR signaling

Membrane binding by CD3ε_{CD} primarily involves electrostatic interactions between basic CD3ε residues and anionic lipids of the inner leaflet of the PM (Aivazian and Stern, 2000; Sigalov et al., 2006; Xu et al., 2008; Deford-Watts et al., 2009). The Grinstein laboratory previously reported a fluorescent probe for assessing the overall negative charge of the inner leaflet of the PM. This anionic lipid probe, termed R-pre, is based on a C-terminal K-Ras sequence responsible for PM targeting (Yeung et al., 2006). Membrane binding by this 18-aa probe requires a cluster of basic residues, as well as a cysteine-linked prenyl group that can partition into the lipid bilayer. This probe was found to primarily label the inner leaflet of the PM, due to a higher negative charge of the PM compared other membranes. A reduction in the number of basic residues resulted in dissociation from the PM, demonstrating

that the prenyl group was not sufficient for PM localization. In vitro assays showed that the R-pre probe strongly bound to anionic lipids, in particular PS (the most abundant anionic lipid of the inner leaflet) and phosphatidic acid (a low-abundance anionic lipid); some binding to PIP₂ was also observed (Yeung et al., 2006).

We introduced a monomeric RFP (mRFP)-tagged version of R-pre (R-pre-mRFP) into B-A8 T cells to examine possible changes in PM lipid composition during early stages of T cell activation (Fig. 4 A). As previously described, the probe primarily localized to the inner leaflet of the PM (Fig. 4, A and C; Yeung et al., 2006). When T cells were activated through the TCR using HA-DR4/ICAM-1 lipid beads, a rapid reduction in R-pre-mRFP fluorescence at the PM was observed within the synapse (Fig. 4, A and B). This decrease was observed soon after T cell-APB contact, and occurred concomitant with an increase in ZAP-70-eGFP fluorescence

at the interface (a peak of ZAP-70 fluorescence was visualized at the interface, despite substantial cytosolic ZAP-eGFP fluorescence; Fig. 4, C and D). It was important to assess the possibility of steric hindrance by recruited signaling molecules. We constructed a control protein that was also anchored to the membrane through a lipid tail: eGFP with an N-terminal myristoylation and dual palmitoylation signals (MyrPalmeGFP). This probe also associated primarily with the inner leaflet of the PM (Fig. 4 E; Hashimoto-Tane et al., 2010). Only small changes in MyrPalm-eGFP fluorescence were observed at the T cell–APB interface when T cells expressing this control protein were stimulated with APB (Fig. 4, E-G).

The formation of TCR microclusters is one of the earliest steps in TCR signaling. Microclusters tend to form at the periphery of the T cell–APC interface and are transported to the center of the synapse (central supramolecular activation cluster; cSMAC), a site of TCR internalization (Yokosuka and

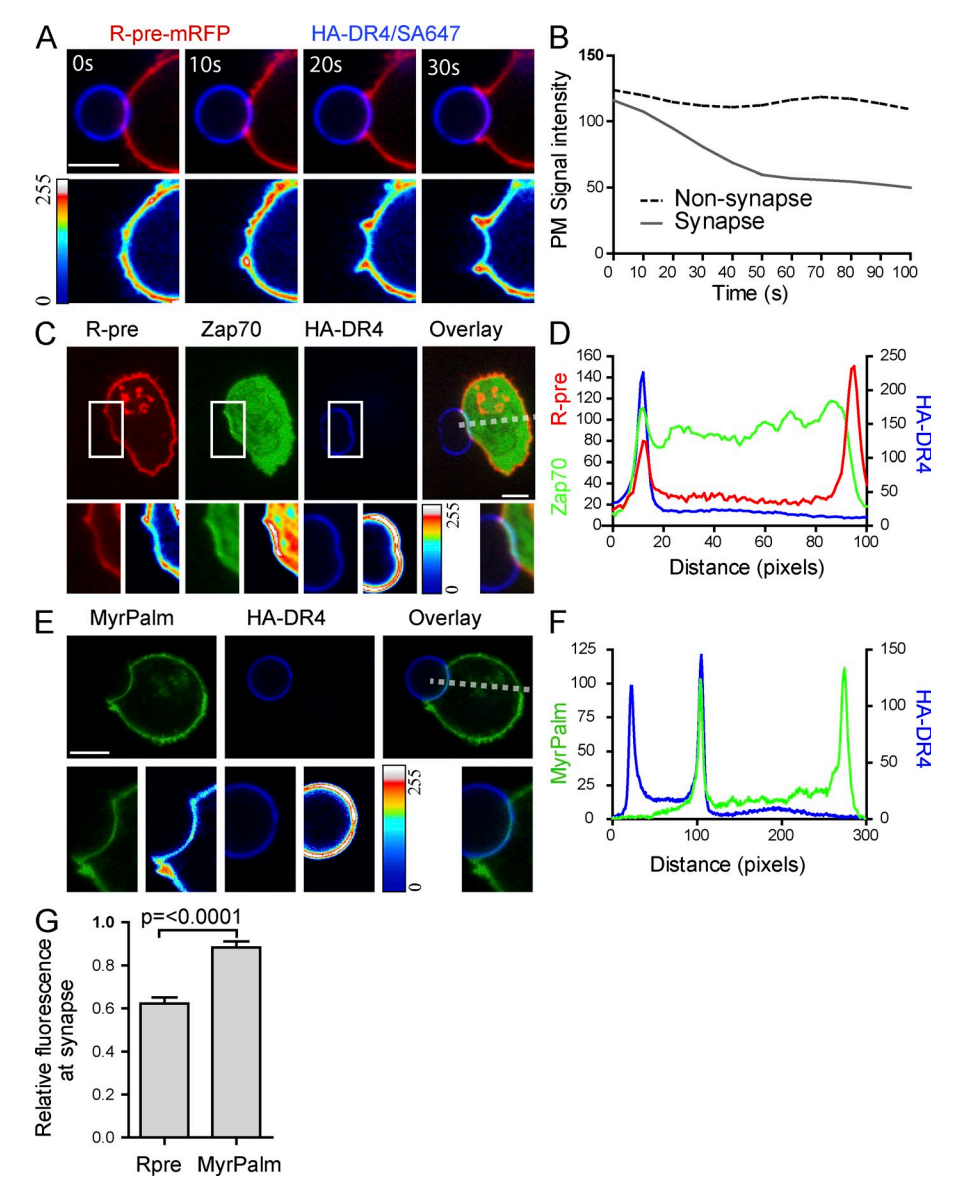


Figure 4. Reduction of negative charge at the inner leaflet of the T cell synapse during early stages of TCR engagement by peptide-MHC. (A and B) B-A8 T cells expressing the anionic lipid probe R-premRFP were stimulated with HA-DR4/ICAM-1 lipid beads and imaged by confocal microscopy at 10-s intervals. Top row: typical cell showing bead (blue) and R-pre binding to inner leaflet (red) as synapse is formed. Bottom row shows intensity of R-pre fluorescence using pseudo-color gradient; quantification within or outside of synapse (B). Images representative of n > 3 experiments. Bar, 5 µm. (C and E) B-A8 T cells expressing both R-pre-mRFP and ZAP-70-eGFP probes (C) or MyrPalm-eGFP probe (E) were stimulated with HA-DR4/ICAM-1 lipid beads and imaged by confocal microscopy. Bottom rows show higher magnification (white box) and pseudo-color gradient of fluorescence intensity. Dotted line represents cross section for cells shown in D and F. Images representative of n > 3 experiments. Bar, 10 µm. (D and F) Fluorescence signals of bead (blue), R-pre (red), and ZAP-70 (green; D) or Myr-Palm (green; F) across cells in C and E (dotted lines). (G) Population analysis of ratio between PM fluorescence within or outside bead-cell interface for at least 30 cells per group, error bars show SEM. P-value was calculated using an unpaired two-tailed Student's t test with a 99% Cl. n > 10 cells per experiment.

Saito, 2010). This process can be imaged at high resolution by TIRF microscopy using the planar lipid bilayer system. We incubated B-A8 T cells expressing R-pre-mRFP on lipid bilayers displaying HA-DR4 (bound to streptavidin-Alexa Fluor 488 [SA-488]) and unlabeled ICAM-1. Interestingly, R-pre-mRFP labeling was reduced in defined spots of the PM that colocalized with TCR microclusters (Fig. 5 A), suggesting that the negative charge of the inner leaflet of the PM was reduced during early stages of TCR signaling. At later time points, a substantial reduction of R-pre-mRFP

fluorescence was also observed in the cSMAC (not depicted). Pearson's correlation coefficient and colocalization analyses revealed that most, if not all, TCR-pMHC microclusters had a reduced R-pre-mRFP fluorescence signal ($r=-0.28\pm0.05$; Fig. 5, B, C, and H). When T cells coexpressing R-pre-mRFP and ZAP-70-eGFP were injected into a flow cell containing lipid bilayers displaying a control DR-peptide complex (DR4-CLIP) and ICAM-1, no microclusters or subsequent reduction in negative charge were observed (Fig. 5 I). The MyrPalm-eGFP probe was used as a control to exclude

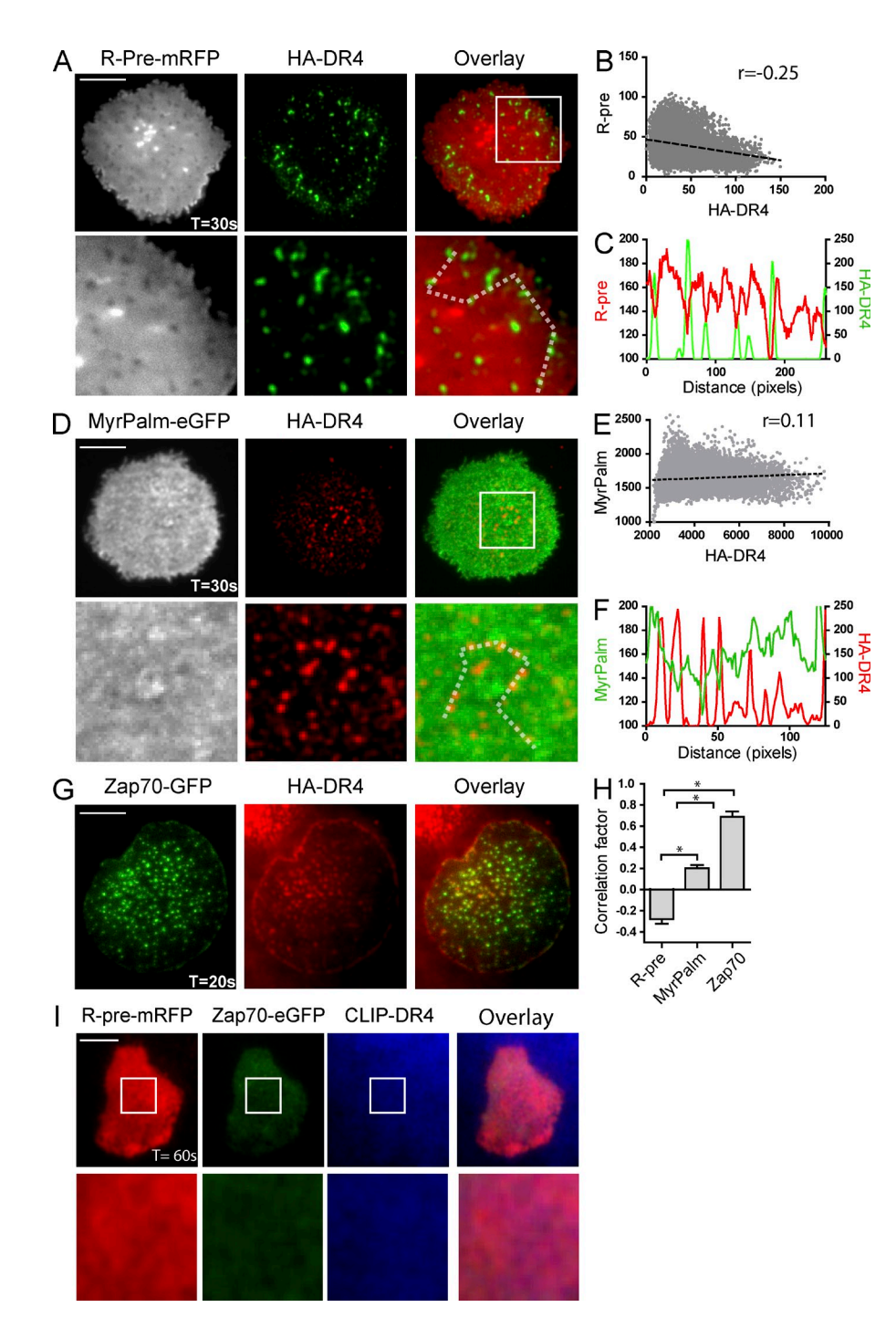


Figure 5. TCR microclusters have a reduced negative charge at the inner leaflet of the plasma membrane. (A and D) B-A8 T cells expressing either R-pre-mRFP (A) or MyrPalm-eGFP (D) probes were imaged on lipid bilayers displaying HA-DR4/ICAM-1 using TIRFM (10-s intervals, 3 min). Higher magnification indicated by inset is shown in bottom panels. Images representative of n > 3experiments. Bar, 10 µm. (B and E) Pearson's correlation coefficient (r) for images in A and D; results of representative images are displayed. (C and F) Fluorescence signal intensities of HA-DR4 microclusters and R-pre-mRFP were measured by connecting several microclusters using line tool (dotted lines in A and D). (G) Recruitment of ZAP-70eGFP to synapse (10-s intervals, 3 min, TIRFM). Images representative of n = 2 experiments. Bar, 10 μm. (H) Population analysis of at least 20 cells per group for fluorophore distribution using Pearson's correlation factor. P values were calculated using unpaired two-tailed t test with 99% CI analysis (*, < 0.00001). n > 10 cells per experiment. (I) T cells expressing R-pre-mRFP and ZAP-70-eGFP were imaged using TIRFM on negative control lipid bilayers displaying CLIP-DR4/ICAM-1. Higher magnification indicated by inset is shown in bottom panels. Images representative of n = 2 experiments. Bar, 10 μ m.

the possibility of steric hindrance, and no reduction in its fluorescence signal was observed in TCR microclusters (Fig. 5, D–F and H). The imaged microclusters were sites of active signaling, as indicated by the substantial accumulation of ZAP-70-eGFP ($r = 0.69 \pm 0.05$; Bunnell et al., 2002; Fig. 5, G and H). Collectively, these results identify early changes in the lipid microenvironment of TCR microclusters.

Reduced density of PS in TCR-pMHC microclusters

The negative charge of the inner leaflet of the PM is largely maintained by PS, which represents \sim 20–30% of total inner leaflet phospholipids (Fridriksson et al., 1999). In live cells,

little PS is present on the cell surface, and this asymmetric distribution is maintained through ATP-dependent lipid flippase activity (aminophospholipid transferase, APLT; Daleke, 2003). All other anionic lipids (phosphatidic acid, different phosphatidylinositol species) are present at low densities. The C2 domain of lactadherin (Lact-C2) was previously shown to bind PS with high specificity, and this interaction does not require calcium (unlike Annexin V); a Lact-C2-mRFP probe was previously used to assess PS distribution during phagocytosis (Yeung et al., 2008). We therefore transduced B-A8T cells with a Lact-C2-mRFP probe, stimulated these cells with either APB or peptide-pulsed live APC (Priess cells), and

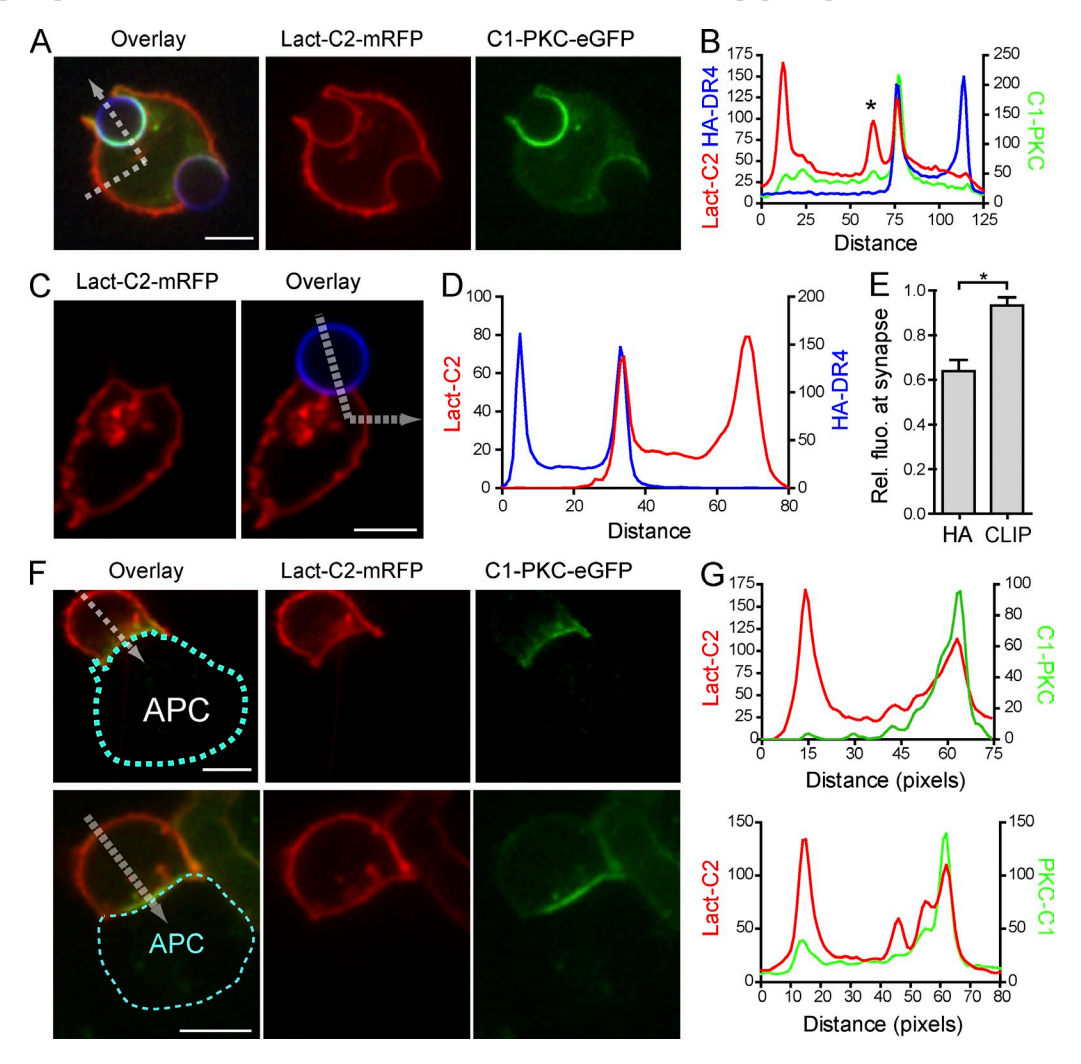


Figure 6. The density of PS is substantially reduced during early stages of synapse formation. (A) T cells expressing a PS probe (Lact-C2-mRFP) and DAG probe (C1-PKC-eGFP) were stimulated with HA-DR4/ICAM-1 lipid beads and imaged by confocal microscopy. Dotted line depicts cross section through cell for quantification shown in B. Images representative of n = 3 experiments. Bar, 5 μm. (B and D) Cross section of fluorescence signal intensity for cells shown in (A and C) at bead-cell contact as well as irrelevant area of PM. Red, Lact-C2; blue, HA-DR4 (SA-647); green, C1-PKC. Asterisk in B indicates Lact-C2 signal from intracellular compartment. (C and D) T cells expressing a PS probe (Lact-C2-mRFP) were stimulated with control CLIP-DR4/ICAM-1 lipid beads and imaged by confocal microscopy. Dotted line depicts cross section through cell for graph in D. Images representative of n = 3 experiments. Bar, 5 μm. (E) Population analysis ($n \ge 30$ cells) of relative fluorescence of Lact-C2-mRFP at synapse for cells stimulated with HA-DR4 or control CLIP-DR4 beads. SEM is shown; *, P < 0.0001. n > 10 cells per experiment. (F) DR4-expressing Priess cells were pulsed with HA peptide (1 μM) for 1 h. T cells were added and imaged by confocal microscopy. Distribution of Lact-C2 and C1-PKC was assessed in stable cell-cell conjugates. Gray dotted line depicts cross section used to generate graph in (G); cyan-colored dotted line depicts Priess cell (APC). Images representative of n = 3 experiments. Bars, 10 μm. (G) Fluorescence signal intensity of probes at cell-cell contact and irrelevant area of cell surface (red, Lact-C2; green, C1-PKC).

imaged synapse formation by confocal microscopy. We also assessed production of diacylglycerol (DAG), which is produced by hydrolysis of PIP₂ by PLC- γ . DAG dynamics were followed using the C1 domain of PKC δ (C1-PKC-eGFP; Codazzi et al., 2001). All APB-stimulated T cells showed a

marked decrease of Lact-C2-mRFP fluorescence at the synapse (Fig. 6, A, B, and E). In contrast, a transient accumulation of the C1-PKC probe was observed at the interface (Fig. 6, A and B). When T cells were instead incubated with APBs displaying the control CLIP-DR4 complex and ICAM-1,

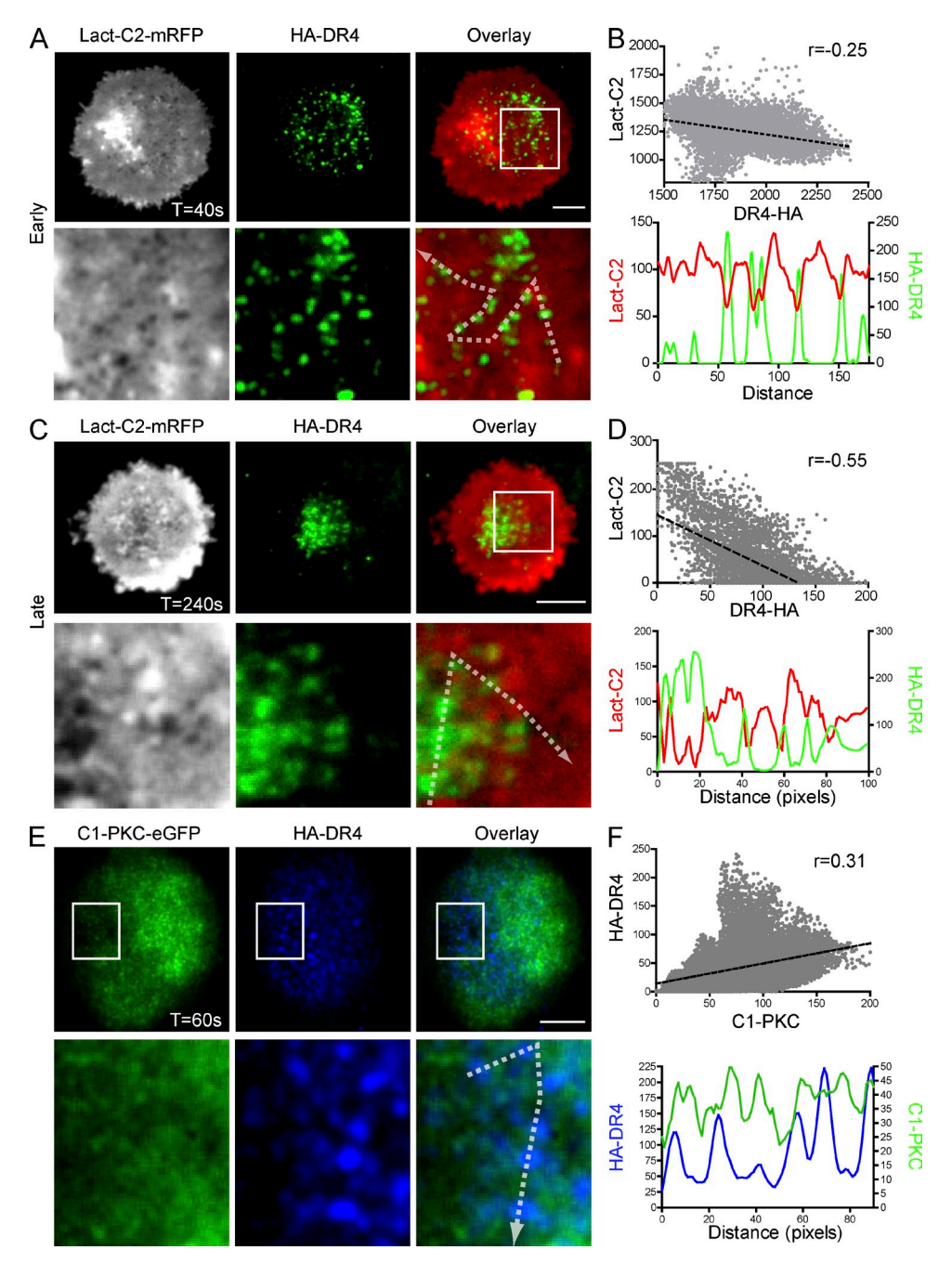


Figure 7. The density of PS is substantially reduced in TCR microclusters during early synapse formation. (A and C) T cells expressing Lact-C2-mRFP were imaged by TIRFM on bilayers displaying HA-DR4/ICAM-1 at 30-s intervals. Early synapse A showing pMHC microclusters and Lact-C2 labeling of PS on inner leaflet of PM. Late synapse C showing cSMAC. Higher magnifications (inset boxes) shown beneath each image. Images representative of n > 3 experiments. Bar, 5 μ m. (B and D) Inset magnifications used to calculate Pearson's correlation coefficient (r), displayed as dot plots. Line tool used to quantify signal intensity of HA-DR4 (green) and Lact-C2 (red), see dotted lines in A and C. (E) T cells expressing C1-PKC-eGFP imaged by TIRFM on bilayers displaying HA-DR4/ICAM-1 (30-s intervals). Early synapse showing pMHC microclusters and C1-PKC labeling of DAG on inner leaflet of PM (top). Higher magnification (inset boxes) shown beneath each image. Images representative of n = 3 experiments. Bar, 5 μ m. (F) Pearson's correlation coefficient (inset box; r), displayed as dot plot. Line tool used to quantify signal intensity of HA-DR4 (blue) and C1-PKC (green) for dotted line in E.

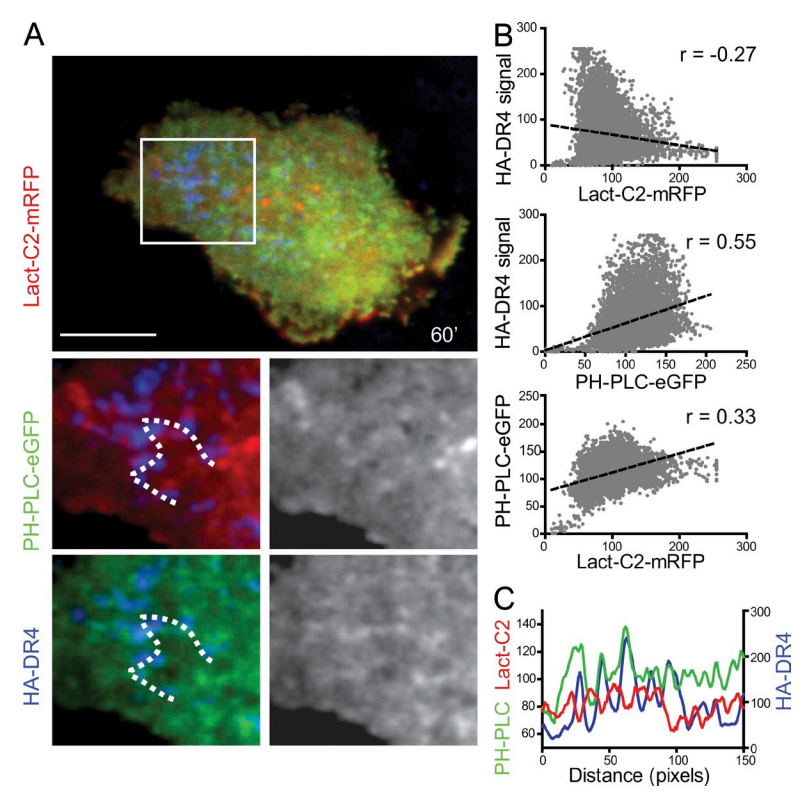


Figure 8. PS, but not PIP2, levels are reduced in microclusters during early synapse formation. B-A8 T cells coexpressing Lact-C2-mRFP and PH-PLC-eGFP were injected into flow cells with lipid bilayers displaying HA-DR4 and ICAM-1. Synapse formation was imaged by TIRFM at 10-s intervals (3 min). (A) Images show early synapse formation (time after T cell contact is indicated in seconds). To simplify visualization, probe signals are also shown in grayscale. Images representative of n = 3 experiments. Bars 10 μ m. (B) Pearson's correlation coefficient calculated for each zoomed image using all fluorophore combinations to examine spatial relationships between distribution of HA-DR4 microclusters, Lact-C2-mRFP, and PH-PLC-eGFP (r, correlation factor). (C) Spatial relationships between HA-DR4 (blue), Lact-C2-mRFP (red), and PH-PLC-eGFP (green) fluorescence were examined by connecting several microclusters (dotted line in A) with line tool.

T cells interacted with the beads but there was little or no reduction of Lact-C2-mRFP at the interface (Fig. 6, C–E). T cells stimulated with peptide-pulsed APC also showed a reduction of PS at the site of cell–cell contact, indicating that observations made with APBs were physiological (Fig. 6, F and G). Thus, the reduction in PS density at the synapse was dependent on pMHC recognition by the TCR.

We next examined distribution of the PS probe in TCR microclusters by imaging T cells on planar lipid bilayers displaying HA-DR4 and ICAM-1 using total internal reflection fluorescence microscopy (TIRFM). A marked decrease in PS density was visualized in newly formed TCR microclusters using the Lact-C2-mRFP probe, and PS content was also reduced later in the cSMAC (Fig. 7, A and C). Co-localization analyses and Pearson's colocalization coefficient revealed a negative correlation between the distribution of PS and TCR-pMHC microclusters (Fig. 7, B and D). A positive correlation was observed between C1-PKC-eGFP distribution and TCR microclusters, indicating that the probe preferentially accumulated in microclusters although it was also distributed over most of the synapse (Fig. 7, E and F). These data showed that TCR microclusters contained lower levels of PS compared with surrounding PM areas, resulting in a reduced negative charge of the inner leaflet.

We further investigated a potential role of PIP_2 hydrolysis as a cause for the observed reduction of negative charge using the pleckstrin homology (PH) domain of PLC δ fused to eGFP (PH-PLC-eGFP; Stauffer et al., 1998). Synapse formation was imaged on planar lipid bilayers, and a marked decrease in PS

content in TCR microclusters was observed, but no significant reduction in the fluorescence signal of PH-PLC-eGFP was noted (Fig. 8 A). Rather, colocalization analyses revealed some enrichment of the PIP₂ probe in TCR microclusters (Fig. 8, B and C). The observation that both DAG and PIP₂ are present and/or enriched in TCR microclusters is consistent with observations on the activation state of enzymes known to rapidly modulate the available pool of PIPs in T cells (Samelson, 2002; Zhang et al., 2009). PIP₂ is hydrolyzed by PLC- γ , phosphorylated to PIP₃ by PI3K, and is also newly synthesized in synapses by phosphatidylinositol 4-phosphate 5-kinase (Sun et al., 2011a).

Inhibition of Lck activity does not prevent local changes in the lipid microenvironment of TCR microclusters

TCR microclusters were previously shown to form when TCR signaling was blocked with the Src kinase inhibitor PP2, which inhibits Lck (Campi et al., 2005). We therefore tested whether changes in lipid composition occur in TCR microclusters when T cells were treated with PP2. B-A8 T cells expressing R-pre-mRFP and ZAP-70-eGFP probes were incubated with lipid beads displaying HA-DR4 and ICAM-1. PP2-blocked T cells formed intimate contacts with the antigen-presenting lipid beads reminiscent of synapse formation (Fig. 9 A) but did not flux calcium (Fig. 9, B and C; and Videos 1 and 2). Also, T cells did not visibly accumulate ZAP-70-eGFP at the T cell-APB contact site, consistent with inhibited Lck activity (cytoplasmic ZAP-70 levels were high, and we could therefore not exclude low-level recruitment of

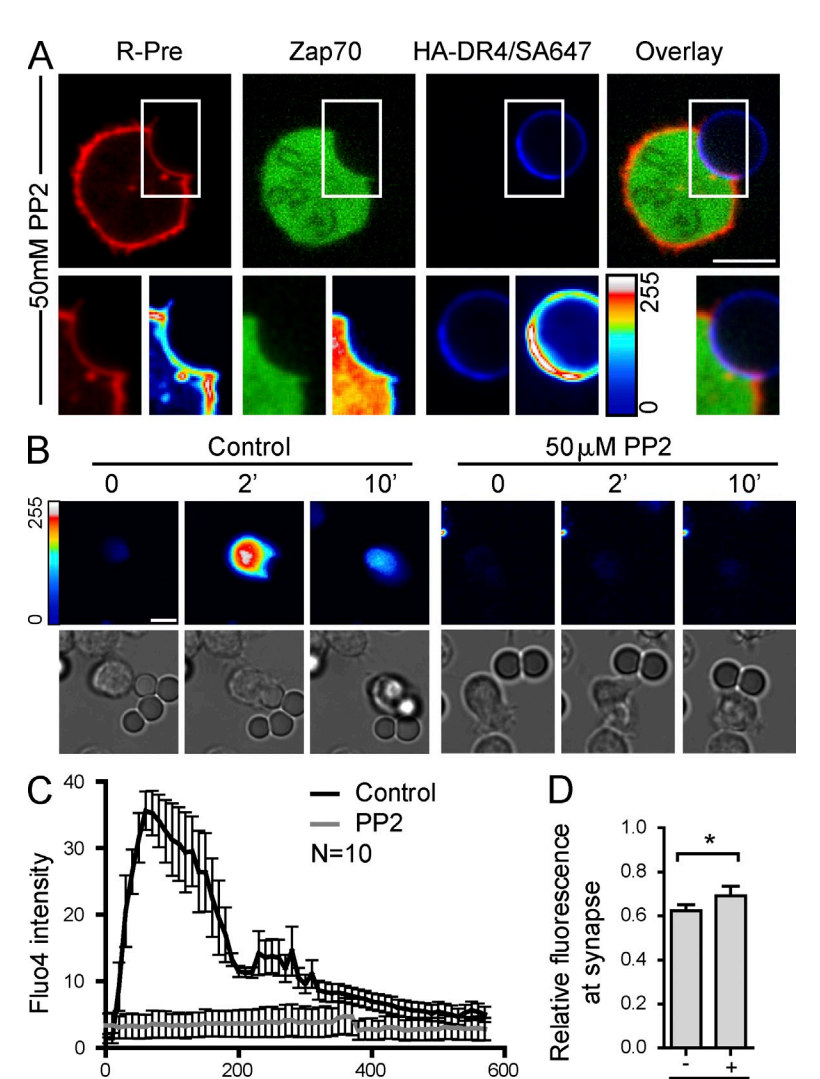


Figure 9. Changes in lipid composition of TCR microclusters occur even when Lck activity is inhibited. (A) B-A8 T cells expressing R-pre-mRFP and ZAP-70-eGFP probes were treated with 50 µM PP2 before and during stimulation with HA-DR4/ICAM-1 lipid beads. Cells were imaged by confocal microscopy (10-s intervals). Bottom row shows higher magnification of bead-cell interface (white box). Images representative of n > 3 experiments. Bar, 10 μ m. (B) WT B-A8 T cells were labeled with calcium probe Fluo-4AM and incubated with or without $\pm 50~\mu M$ PP2 treatment. Cells were then stimulated with HA-DR4/ICAM-1 lipid beads \pm PP2. Calcium flux was imaged during bead stimulation (10-s intervals, 10 min) by wide-field microscopy. Typical cells for each condition are shown at three time points. (top row) Intensity of Fluo-4 signal in pseudo-color gradient. (bottom row) DIC images at same time points. Bars, 10 μm. (C) Fluo-4 intensities during bead stimulation $\pm PP2$ treatment (n = 10cells per time point). Data representative of n = 3 experiments. (D) Population analysis of relative R-pre fluorescence intensities at PM of bead-cell interface versus irrelevant membrane for cells stimulated with HA-DR4/ICAM-1 lipid beads \pm treatment with 50 μ M PP2 ($n \ge 30$ cells). P-value was calculated with an unpaired two-tailed Student's t test with a 99% CI (*, 0.0237). n = 10 cells per experiment.

ZAP-70). Nevertheless, a substantial reduction in R-pre-mRFP fluorescence was observed at the interface for all cells, as in cells not treated with this inhibitor (Fig. 9, A and D).

Time (s)

We next examined PS localization in TCR microclusters when Src kinases were inhibited with PP2. T cells were imaged by TIRFM on planar lipid bilayers displaying HA-DR4 and ICAM-1. Control T cells formed typical microclusters, whereas PP2-treated T cells accumulated much larger patches of pMHC while maintaining a small footprint on the bilayer (Fig. 10 A). The morphology of pMHC-TCR patches under PP2 treatment differed somewhat from a previous study (Campi et al., 2005); the difference is possibly related to variances between human and mouse T cells, TCR affinities, or densities of pMHC/ICAM-1. However, our data do confirm that TCR clustering does occur when Src kinase activity is inhibited with PP2. Interestingly, a decrease in PS density was observed in PP2-treated cells at the PM where pMHC was clustered (Fig. 10 A). Pixel-by-pixel colocalization analyses confirmed these observations and showed an average Pearson's

coefficient value of -0.21 ± 0.03 SEM. This value was similar to B-A8 T cells that were activated in the absence of PP2 ($r = -0.26 \pm 0.05$ SEM; P = 0.357; Fig. 10, B and C). The presence of TCR in the large pMHC patches observed in PP2-treated T cells was confirmed by imaging CD3 ϵ -YF-TFP cells under the same conditions (Fig. 10 D). These results demonstrated that TCR clusters have reduced densities of PS even when signaling is inhibited with a Src kinase inhibitor.

Reduced lateral diffusion of PS in synapses

The observation that changes in lipid composition of TCR microclusters occur even in the absence of signaling suggested a nonenzymatic mechanism. We investigated diffusion of PS inside and outside of synapses using fluorescence recovery after photobleaching (FRAP) for a PS probe (Lact-C2), an anionic charge probe (R-pre), and a negative control (MyrPalm). In these experiments, we photobleached defined membrane areas within and outside of synapses, and then monitored the kinetics of fluorescence recovery caused by

JEM Vol. 209, No. 13 2433

50 μM PP2

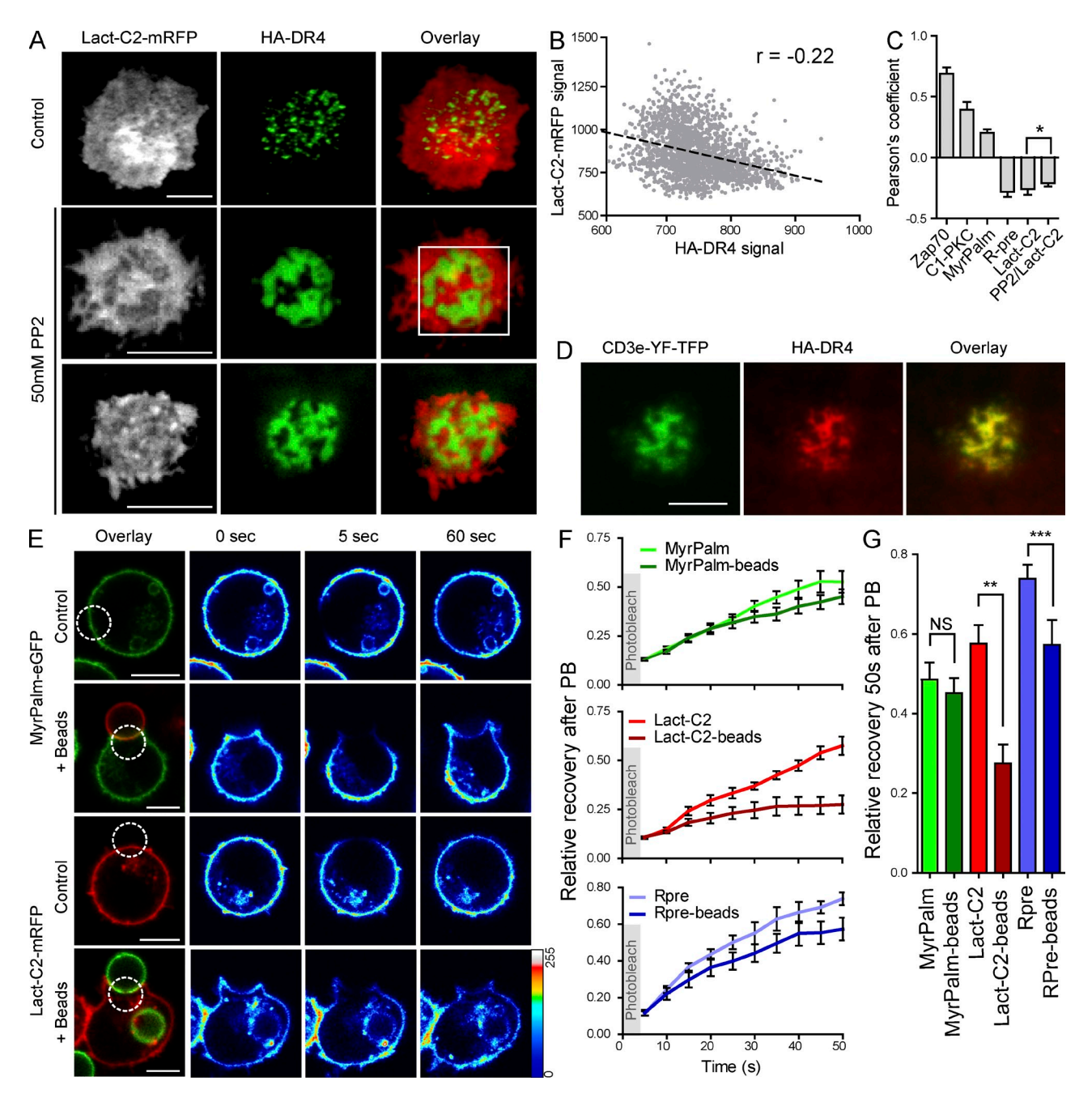


Figure 10. TCR-pMHC microclusters have a reduced density of PS even when Lck activity is blocked. (A) B-A8 T cells expressing PS lipid probe Lact-C2-mRFP were treated $\pm 50 \, \mu$ M PP2 and injected into flow cell with HA-DR4/ICAM-1 lipid bilayers. T cells were imaged using TIRFM at 30-s intervals for 5 min. (top row) Control cells show distinct TCR-pMHC microclusters (green), correlated with reduced Lact-C2 signal in these microclusters (red). (bottom rows) PP2-treated cells show larger pMHC-TCR clusters (green), again correlated with reduction in Lact-C2 signal in these clusters (red). Images representative of n=3 experiments. Bars, 10 μm. (B) Pearson's correlation graph of bottom cell in A treated with PP2. (C) Population analysis of at least 20 cells per group assessed for all tested lipid probes including the PP2 treatment experiment in A. Pearson's correlation factor was calculated by plotting fluorescence signals from lipid probes against HA-DR4 signal using a ROI encompassing only the synapse; correlation factors were plotted as bar graph. P-value was calculated using an unpaired two-tailed Student's t test with a 99% CI analysis (*, P = 0.357). n > 20 cells per group. (D) B-A8 T cells expressing CD3 ϵ -YF-TFP were treated with 50 μM PP2 and imaged by TIRFM on HA-DR4/ICAM-1 bilayers. Images representative of n=3 experiments. Bar, 10 μm. (E) B-A8 T cells that expressed Lact-C2-mRFP, R-pre-mRFP, or MyrPalm-eGFP were imaged for FRAP analysis at the plasma membrane of resting or HA-DR4/ICAM-1 lipid bead-stimulated cells. FRAP was performed at site of synapse for stimulated cells. An area of membrane opposite to FRAP region was selected for normalization. Images are representative for each condition. Region of interest (ROI) is depicted as dotted circle. Images on the right show fluorescence intensities as pseudo-color gradient. Images representative of n=3 experiments. Bars, 5 μm. (F) FRAP during course of image acquisition (50 s). Results are shown as ratio between fluorescence level of oppos

lateral diffusion of fluorescent molecules into the photobleached area. We first performed FRAP on nonstimulated T cells and compared the fluorescence recovery of Lact-C2-mRFP, R-pre-mRFP, and MyrPalm-eGFP (Fig. 10, E–G). Fluorescence recovery of Lact-C2 was reduced when compared to R-pre, as previously observed by Kay et al. (2012) in a comparison of Lact-C2 and tk-Kras-GFP (which is similar to the R-pre probe; Fig. 10, F and G). When T cells were stimulated with lipid beads displaying pMHC and ICAM-1, recovery of Lact-C2 fluorescence in the synapse was substantially reduced compared with nonstimulated T cells (Fig. 10, F and G). The recovery of R-pre fluorescence was also reduced, but to a lesser extent. In contrast, no statistically significant differences were observed for the MyrPalm probe at any time point.

Indeed, at the 50-s time point, the Lact-C2 mobile fraction was drastically reduced in synapses of activated cells (0.28 \pm 0.0466 SEM) compared with nonstimulated cells (0.58 \pm 0.0467). Also, a significant reduction (P = 0.029) of the mobile fraction was observed for R-pre (from 0.74 \pm 0.045 in nonstimulated cells to 0.57 \pm 0.062 in synapses of stimulated cells). No significant changes were observed for the MyrPalm probe (0.49 \pm 0.043 and 0.45 \pm 0.039 for nonstimulated cells and synapses of stimulated cells, respectively).

DISCUSSION

These data identify a mechanism for release of the CD3 ϵ cytoplasmic domain from the PM after TCR triggering. FRET measurements based on fluorescence lifetime microscopy (FLIM) demonstrated membrane binding by CD3 $\varepsilon_{\rm CD}$ in live human T cells. After TCR engagement of pMHC complexes, the plasma membrane at the synapse had a reduced binding capacity for CD3 $\epsilon_{\rm CD}$. A series of probes for defined lipid species enabled visualization of local changes in lipid composition of the inner leaflet in TCR microclusters, specifically a reduced negative charge (R-pre probe) and a lower density of the most abundant anionic PM lipid, PS (Lact-C2 probe). These changes in lipid composition were observed as soon as TCR microclusters were detected. Interestingly, the local PS density was reduced even when Lck was inhibited with PP2. No calcium flux was detected in such cells, indicating that traditional TCR signaling cascades are not required for these local changes in lipid composition. We consider it unlikely that the observed changes in lipid composition of TCR microclusters are related to formation of 'lipid rafts'. Indeed, a recent study by the Saito group showed that TCR microclusters are formed independently of lipid raft clustering: FRET microscopy showed no colocalization between TCR microclusters and several fluorescent raft probes, including the cholera toxin B subunit (Hashimoto-Tane et al., 2010).

It was important to exclude steric hindrance of the probes as an explanation for these results. A negative control protein (lipid anchored MyrPalm-eGFP) was not excluded from TCR microclusters; also, a fluorescent probe for DAG, an important lipid involved in TCR signaling, showed substantial accumulation at the synapse. Steric hindrance by recruited

signaling molecules was unlikely in experiments involving inhibition of Lck by PP2 treatment.

Several groups have shown that the CD3 ε and ζ cytoplasmic domains bind to the plasma membrane and that these interactions are primarily driven by interactions between negatively charged lipid headgroups and clusters of basic residues of CD3 ε and ζ . Because of the electrostatic nature of these interactions, multiple anionic phospholipids can contribute to membrane binding, including PS and phosphatidylinositol species (Aivazian and Stern, 2000; Sigalov et al., 2006; Xu et al., 2008; DeFord-Watts et al., 2009, 2011; Zhang et al., 2011). A previous NMR structure of the CD3ε cytoplasmic domain also demonstrated that all hydrophobic residues, including all aliphatic residues and the two tyrosine residues of the ITAM, partition into the hydrophobic core of the bilayer (Xu et al., 2008). The NMR structure identified a dynamic binding mode which may be relevant for release from the membrane. Changes in the lipid composition of TCR microclusters, as identified here, may shift the equilibrium and substantially reduce the fraction of CD3ε cytoplasmic domains that are membrane bound. FRET-FLIM imaging indeed demonstrated substantially reduced membrane binding of the CD3ε-YF-TFP probe at the synapse after pMHC recognition, even though the cytoplasmic domain of this probe could not be phosphorylated.

A recent study proposed that dissociation of the ζ chain from the PM occurs after phosphorylation (Zhang et al., 2011). In this study, TCRs were activated with CD3 antibodies rather than pMHC ligands. The CD3 ε ITAM is located close to the C terminus to which the TFP reporter protein was attached for FRET-FLIM measurements. In contrast, the ζ chain has three ITAM segments and a C-terminal fluorescent protein cannot report with the same degree of fidelity on the binding state of the first two ITAM segments of the ζ chain. Not all CD3 ITAMs may detach simultaneously from the membrane, and transient release of one ITAM may result in its phosphorylation by Lck. Introduced negatively charged phosphate groups have been shown to interfere with ζ membrane binding (Aivazian and Stern, 2000; Sigalov et al., 2006). Phosphorylation of one of the ITAMs may thus be sufficient to shift the equilibrium toward the unbound state.

PS is considerably more abundant than all other anionic lipids on the inner leaflet of the PM (\sim 20–30% for PS, \sim 1% for PIP₂ and considerably less for other anionic phospholipids; Fridriksson et al., 1999). Imaging experiments demonstrated a reduced density of PS within TCR microclusters (Lact-C2 probe), along with a reduced negative charge (R-pre probe). Both changes occurred with similar kinetics and had a similar distribution; a reduced density of both probes was also observed in TCR clusters in the presence of the PP2 inhibitor. Dynamic changes in phosphatidylinositol content are also known to occur during TCR activation. PIP2 hydrolysis by PLC-y results in a loss of its negative charge. However, PIP₂ is also synthesized in synapses by phosphatidylinositol 4-phosphate 5-kinase and transient PIP₂ accumulation can occur early during synapse formation (Sun et al., 2011a). Consistent with these findings, we observed some enrichment of a PIP₂

probe (PH domain of PLCδ) in early TCR microclusters, yet a reduced PS density in the same microclusters. Yeung et al. (2006, 2008) have identified substantial changes in lipid composition of phagosomes. Interestingly, PS content was not reduced in phagocytic cups or fully formed phagosomes (Yeung et al., 2009). However, a substantial reduction in negative charge of phagosomal membranes, which correlated with PIP₂ hydrolysis, was visualized with the R-pre probe (Yeung et al., 2006). Thus, substantial changes in the charge of the inner leaflet are observed in both TCR microclusters and phagosomes, but there are differences in the mechanisms.

The Lact-C2 probe detects free PS, which is the relevant form for determining charge and, consequently, the membrane-binding behavior of the CD3 ϵ cytoplasmic domain. The probe does not detect PS that is bound by other proteins and thus inaccessible to the Lact-C2 and R-pre probes we used. Thus, it is possible that other proteins in TCR microclusters bind a fraction of available PS, thereby reducing the local negative charge of the inner leaflet of the PM. It is important to note, however, that Lact-C2 has a high affinity for PS (K_d of 3.4 nM; Shi et al., 2004; Yeung et al., 2008) and that a reduction of Lact-C2 and R-pre binding in TCR microclusters is observed even when TCR signaling is inhibited by treatment with PP2. Recruitment of such other PS-binding proteins to TCR microclusters would thus have to occur even in the absence of signaling.

The FRAP data showed reduced lateral diffusion of PS in synapses formed by T cells interacting with lipid beads displaying mobile pMHC and ICAM-1. These experiments measured recovery of Lact-C2 and R-pre fluorescence after photobleaching at the entire synapse because individual TCR microclusters are very difficult to visualize when T cells are stimulated with APC or beads carrying pMHC ligands for the TCR. Thus, these data represent a mean of fluorescence recovery at the interface, within and outside of TCR microclusters. Previous work showed that a sizable fraction of PS in the plasma membrane has limited mobility (Kay et al., 2012). Experiments in HeLa cells identified a mobile fraction of only 0.43, and our experiments in nonstimulated T cells showed a mobile fraction of 0.58 (the relatively small difference may be cell-type related). Interestingly, the mobile PS fraction was greatly reduced in synapses (to 0.28). Previous work has implicated the cytoskeleton in reducing the mobile fraction of PS; treatment of cells with jasplakinolide, an actin stabilizer that induces the formation of blebs as the cytoskeleton contracts, increased the mobile fraction to 0.93 in actin-free membrane areas (Kay et al., 2012). EM studies further showed that PS has a nonhomogenous distribution in the plasma membrane, with a substantial fraction in nanoclusters with a diameter of \sim 11 nM (Fairn et al., 2011).

Finally, it remains possible that enzymatic mechanisms contribute to the reduced density of PS in TCR microclusters. However, we think that a nonenzymatic mechanism is more likely, given that the changes in lipid composition occurred even when the most proximal enzyme in the TCR signaling cascade (Lck) was pharmacologically inhibited. The following

enzymatic mechanisms could be envisioned: (a) Calcium flux activates a scramblase that can disrupt lipid asymmetry between the inner and outer leaflet of the PM (Suzuki et al., 2010). However, our data show that the local changes in lipid composition of TCR microclusters occur even when Lck kinase activity is blocked. (b) The asymmetric distribution of PS between the outer and inner leaflet is maintained by a lipid flippase (APLT), and local inhibition or exclusion of this flippase could result in loss of PS from TCR microclusters (Folmer et al., 2009). (c) PS can be decarboxylated in mast cells after activation by concanavalin A (Hirata et al., 1979; Schuiki and Daum, 2009). Decarboxylation removes the negative charge and converts PS to phosphatidylethanolamine.

The described changes in the lipid microenvironment of TCR microclusters may not only result in release of CD3 ϵ (and ζ) cytoplasmic domains from the plasma membrane, but also serve other functions in TCR microclusters. For example, a reduction of the negative charge may facilitate the recruitment of signaling molecules to the inner leaflet of the plasma membrane in TCR microclusters or later contribute to TCR internalization in the cSMAC (Vardhana et al., 2010).

MATERIALS AND METHODS

Reagents. Anti–CD3ζ(pY142) antibody was purchased from BD, anti–human CD3ζ (6B10.2) was obtained from Santa Cruz Biotechnology, anti–phosphotyrosine (p-Tyr-100) was purchased from Cell Signaling Technology, and mouse IgG was obtained from Jackson ImmunoResearch Laboratories. Isotype antibodies mouse IgG2a, κ (MOPC-173) and mouse IgG1κ (MOPC-21), anti–human CD2 (RPA-2.10), anti–human CD3 (UCHT1), anti–human CD4 (OKT4), anti–human CD11a/LFA-1 (HI111), anti–human CD54/ICAM1 (MEM-111), anti–human CD69 (FN50), and anti–human CD80 (2D10) were obtained from BioLegend. Src-kinase inhibitor PP2 was purchased from EMD. Fluo-4AM was obtained from Invitrogen.

Plasmids. All lentiviral constructs were made using the pHAGE-fullEF1a lentiviral vector (provided by Vector Core, Dana-Farber/Harvard Cancer Center). The Lact-C2 and R-pre constructs were a kind gift from S. Grinstein (The Hospital for Sick Children, Toronto University, Toronto, Canada). C1-PKC-eGFP and PH-PLC-eGFP constructs were purchased from Addgene. Other constructs with fluorescent reporter proteins were generated by overlapping PCR.

Lentivirus production. HEK-293T cells (American Type Culture Collection) were cultured in DMEM media supplemented with 10% FBS, 2 mM GlutaMAX-I (Invitrogen) and 10 mM Hepes (complete DMEM media). Cells were passaged the day before infection to achieve \sim 70% confluence at infection. Cells were transfected with the lentivirus triad of plasmids DR8.91, pMSCV-VSV-G, and pHAGE using TransIT express transfection reagent (Mirus) according to the manufacturer's protocol. For 3 consecutive days, supernatant was harvested and replaced with 12 ml of complete DMEM media. Supernatants (3 \times 12 ml) were pooled, filtered (0.45 μ m), and virus was pelleted by ultracentrifugation. Concentrated virus was recovered and aliquots were snap-frozen in liquid nitrogen. Viral titers were determined using the human Jurkat cell line.

T cell culture and lentiviral infection. T cell clone BA-8 was isolated from PBMCs of a healthy donor using tetramers of HA₃₀₆₋₃₁₈ peptide and HLA-DR4 (Schubert et al., 2012). T cells were grown in RPMI-1640 supplemented with 10% FBS, 1% human serum (Valley Biochemical), 2 mM GlutaMAX-I, 10 mM Hepes (all Invitrogen), and 5 U/ml rIL-2 (Roche; T cell media). T cells were restimulated in 2-wk intervals with PHA-L (Roche),

irradiated human PBMCs, and rIL-2, as previously described (Wucherpfennig et al., 1994).

For lentiviral transduction, a spin infection method was used on day 8 after stimulation. In brief, 2×10^6 T cells were resuspended in 500 μ l of supplemented RPMI media containing 8 $\mu g/ml$ of polybrene and lentivirus (20:1 multiplicity of infection). Cells were incubated with the virus for 30 min at 37°C in 24-well plates coated with 50 $\mu g/ml$ of retronectin (Takara) for 24 h at 4°C before infection. Spin infection was performed at 2,000 rpm at 30°C for 90 min. After centrifugation, cells were incubated for 1 h at 37°C, and 2 ml of T cell media was then added. The next day, cells were washed and cultured for an additional 5 d in T cell media. On day 14 after stimulation, cells were sorted by flow cytometry based on expression of fluorescent reporters, and then restimulated and cultured as described above. T cells were typically used between days 7 and 10 for all experiments.

Expression of DR4 and ICAM-1 molecules for synapse imaging. Soluble murine ICAM-1 with a C-terminal His₁₂-tag was produced from stably transfected Schneider cells (S2) and purified using an anti–ICAM-1 (YN1/1.7.4) affinity matrix followed by a Ni-NTA column (Dustin et al., 2007). ICAM-1 was labeled with Alexa Fluor 647 (Invitrogen) and purified using a Ni-NTA column.

Soluble HLA-DR4 (*DRA*, *DRB1**04:01) was produced using a CHO cell transfectant in a hollow fiber bioreactor (Day et al., 2003). HLA-DR4 protein was expressed with a CLIP peptide covalently linked to the N terminus of the DR β -chain via a thrombin-cleavable linker and a C-terminal BirA-tag (DR α chain) for site-specific biotinylation. HLA-DR4 was affinity purified using an anti-DR (L243) matrix. Biotinylation of the BirA site was performed as previously described (Day et al., 2003). The CLIP linker was cleaved with thrombin, and peptide loading was performed overnight at 30°C in citrate-buffered saline (pH 5.2) in the presence of EDTA (1 mM), protease inhibitors, and the small molecule J10 that accelerates peptide loading (Call et al., 2009). HA₃₀₆₋₃₁₈ peptide used in the loading reaction was synthesized with a C-terminal DNP group on an introduced lysine. Peptide–DR complexes were finally purified using a Superose 12 gel filtration column (GE Healthcare) and an anti-DNP affinity matrix.

T cell synapse formation on lipid bilayers using TIRFM. Glass-supported planar lipid bilayers were generated by applying DOPC liposomes containing 15% Ni-NTA-DGS and 0.05% cap-biotin-PE lipids (all Avanti Polar Lipids) on acid-washed coverslips that were placed into a FCS2 flow cell (Bioptechs; Dustin et al., 2007). Flow cells were flushed with Hepes-buffered saline supplemented with 6 mM glucose, 2 mM MgCl₂, 1 mM CaCl₂, and 1% human serum albumin (HBS/HSA; SeraCare Life Sciences). Lipid bilayers were blocked with 5% casein in PBS containing 100 µM NiCl₂. Polyhistidine-tagged ICAM-1 (~200 molecules/μm²) was captured onto bilayers by binding to Ni-NTA-DGS lipids. Mono-biotinylated pMHC (40 molecules/µm²) was captured by streptavidin (Alexa Fluor 488 or 568 labeled; Invitrogen), which had first been bound to cap-biotin on the bilayers. Protein densities were determined as previously described (Schubert et al., 2012). T cells were cultured for 2-3 h in the absence of IL-2 before application to lipid bilayers. In some experiments,T cells were treated with the Src kinase inhibitor PP2 (50 µM; EMD) for 45 min at 37°C in HBS/HSA buffer, and then directly applied to bilayers.

TIRFM imaging was performed on an inverted Nikon Ti-E microscope equipped with motorized control of a TIRF laser illumination unit. All TIRF images were acquired through a 100× Apo TIRF NA 1.49 oil objective. TIRF imaging was done with excitation from solid state lasers delivered through a single optical fiber into the TIRF arm (Andor) and a quad-bandpass TIRF filter set. Fluorescence emission was captured though single bandpass emission filters mounted in a filter wheel on the side port, just upstream of a 14-bit Clara Interline High-Resolution CCD Camera (Andor Technology). TIRF angle alignment, optimized for each laser line, was performed following the manufacturer's instructions.

Imaging of T cell synapse formation by confocal microscopy. Antigenpresenting lipid beads (APB) were prepared as follows. Nonfunctionalized silica beads (Bangs Laboratory) were washed twice in Ringer's solution and then incubated for 10 min with 0.4 mM DOPC liposomes containing 15% Ni-NTA-DGS and 0.05% cap-biotin-PE lipids (same composition as planar lipid bilayers). Beads were washed twice and then blocked with casein for 10 min. After the beads had been washed twice in Ringer's solution, streptavidin-Alexa Fluor 647 (5 μ g/ml), mono-biotinylated HA-DR4 (1 μ g/ml), and ICAM-1-His $_{12}$ (3 μ g/ml) were captured onto the beads sequentially for 10 min with two washes with Ringer's solution between steps. The final bead stock solution was resuspended in HBS/HSA before injection into flow cells.

DR4-expressing Priess (DRA, DRB1*04:01) cells were cultured in RPMI-1640 supplemented with 10% FBS, 2 mM GlutaMAX-I and 10 mM Hepes. Priess cells were pulsed with 1 μ M peptide for 3 h, washed, and resupended in Ringer's solution. T cells were injected into a laminar flow chamber FCS2 (Bioptechs) containing an acid-cleaned coverslip to immobilize the T cells. Priess cells or lipid beads were then injected (HBS/HSA) and allowed to interact with T cells. Conjugates were imaged using a spinning disk confocal microscope, an inverted Nikon-Ti-E microscope with Perfect Focus system and Prior Stage systems. All images were acquired using a $100\times$ plan-Apo NA 1.40 objective, single laser and bandpass filters, and captured with the 12-bit ORCA-ER CCD camera (Hamamatsu).

Fluorescence lifetime imaging and FRET. Transduced B-A8 T cells expressing CD3 ϵ -YF-TFP were cultured before imaging, in the absence of IL-2 for 2 h. T cells were resuspended in PBS at 10 6 cells/ml, and 100 μ l was loaded into a RH20 flow cell (Harvard Apparatus) containing an acid-washed coverslip. Cells were left to adhere for 5 min before 200 μ l of HBS/HSA solution (kept at 37°C) \pm APBs was injected at 0.5 ml/min using a syringe pump. Cells were incubated an additional minute at room temperature, and cold PBS was then continuously injected for 2 min at 0.3 ml/min. This was followed by injection of 800 μ l of the R18 acceptor fluorophore (2 μ g/ml in cold PBS) at 0.5 ml/min. After labeling of the PM with R18, the cells were continuously washed with cold PBS, pausing only during image and FLIM acquisition.

The flow cell was mounted on an LSM710 upright microscope and observed using a 63× water dipping lens. Confocal images were acquired using single-photon lasers, Ar-458 for mTFP, and HeNe-561 for R18. Emission of fluorescence was detected using spectral detectors with a 60 nm bandwidth, 466-526 nm for mTFP1 and 570-630 for R18. Sample acquisition for FLIM was done using a Coherent Chameleon Vision 2 using a 140 femto second pulse at a 80 MHz pulse rate, laser intensity set at 6%, and a wavelength of 820 nm. The sample was continuously scanned for 40 s using a pixel dwell time of 0.79 ms and a 487-ms frame rate as to minimize donor fluorophore photobleaching during acquisition. These settings typically yielded 3×10^4 – 4×10^5 photons per second, which were detected using the Becker & Hickl TCSPC hybrid module mounted on the microscope and a deflection plate to redirect emitted light toward the detectors. Data generated by the software were saved, and then exported to SPCImage (Becker & Hickl) for analysis. Determination of fluorescence lifetime of PM-targeted CD3ε-YF-TFP was done with a pixel-by-pixel analysis using single exponential curve fitting where the χ^2 was nearest to 1.00 (mean of 1.01 \pm 0.01, n = 25). For FLIM determination of FRET, single and dual exponential decay curve fitting were used to calculate overall FLIM and to determine the fraction of donor fluorophore in the FRET state. Curve fittings typically had a higher χ^2 when single exponential fitting was used in the calculation of overall FLIM in the FRET experiments, an indication of the presence of more than one population of fluorophores with different fluorescence lifetimes. Processed data analysis was done using Prism (GraphPad).

FRAP experiments. Cells were loaded into the RH20 flow cell, as described in the previous section, and imaged using an LSM710 microscope (Carl Zeiss). Cells were either imaged immediately or after activation with antigen-presenting lipid beads. Cells expressing R-pre-mRFP and Lact-C2-mRFP were imaged using the 561 laser line, and fluorescence was captured using 570–630-nm spectral detection. MyrPalm-eGFP-expressing cells were imaged using the 488-nm laser line (497–557-nm spectral detection). Cells were imaged every 5 s for a total of 50 s. For photobleaching, an area of the

plasma membrane was determined using a circular ROI tool encompassing 50 pixels in diameter. Photobleaching of the ROI began immediately after the acquisition of the first image using the zoom bleach method and lasted between 2–4 s, depending on the fluorophore. Typically, 90% of photobleaching was achieved for all fluorophores during this time frame.

FRAP kinetics were calculated based on fluorescence reappearance within the ROI after photobleaching and was compensated for overall photobleaching of the sample during repeated imaging (using an ROI of the plasma membrane opposite to the photobleaching ROI on the same cell). The initial ratio between the two ROIs was set to 1.0 and was used for normalization of all measurements.

Image processing, analysis, and statistical analysis. All images were processed and analyzed using *ImageJ* software. Statistical analysis was performed using Prism (GraphPad).

Online supplemental material. Videos 1 and 2 show WT B-A8 T cells labeled with calcium probe Fluo-4AM 6. Online supplemental material is available at http://www.jem.org/cgi/content/full/jem.20120790/DC1.

We would like to thank Dr. Lisa Cameron for helpful advice, Dr. Mike Dustin for ICAM-1 transfectants, and Dr. Sergio Grinstein for plasmid vectors.

This work was supported by grants from the National Institutes of Health (RO1Al054520 and PO1Al045757 to K.W. Wucherpfennig) and fellowships by the Cancer Research Institute (to E. Gagnon, D.A. Schubert, and H.H. Chu).

The authors have no competing financial interest in this work.

Submitted: 12 April 2012 Accepted: 5 October 2012

REFERENCES

- Aivazian, D., and L.J. Stern. 2000. Phosphorylation of T cell receptor zeta is regulated by a lipid dependent folding transition. *Nat. Struct. Biol.* 7:1023–1026. http://dx.doi.org/10.1038/80930
- Balagopalan, L., N.P. Coussens, E. Sherman, L.E. Samelson, and C.L. Sommers. 2010. The LAT story: a tale of cooperativity, coordination, and choreography. *Cold Spring Harb. Perspect. Biol.* 2:a005512. http://dx.doi.org/10.1101/cshperspect.a005512
- Bunnell, S.C., D.I. Hong, J.R. Kardon, T. Yamazaki, C.J. McGlade, V.A. Barr, and L.E. Samelson. 2002. T cell receptor ligation induces the formation of dynamically regulated signaling assemblies. J. Cell Biol. 158:1263–1275. http://dx.doi.org/10.1083/jcb.200203043
- Call, M.J., X. Xing, G.D. Cuny, N.P. Seth, D.M. Altmann, L. Fugger, M. Krogsgaard, R.L. Stein, and K.W. Wucherpfennig. 2009. In vivo enhancement of peptide display by MHC class II molecules with small molecule catalysts of peptide exchange. J. Immunol. 182:6342–6352. http://dx.doi.org/10.4049/jimmunol.0803464
- Campi, G., R. Varma, and M.L. Dustin. 2005. Actin and agonist MHC-peptide complex-dependent T cell receptor microclusters as scaffolds for signaling. J. Exp. Med. 202:1031–1036. http://dx.doi.org/10.1084/jem.20051182
- Choudhuri, K., D. Wiseman, M.H. Brown, K. Gould, and P.A. van der Merwe. 2005. T-cell receptor triggering is critically dependent on the dimensions of its peptide-MHC ligand. *Nature*. 436:578–582. http:// dx.doi.org/10.1038/nature03843
- Codazzi, F., M.N. Teruel, and T. Meyer. 2001. Control of astrocyte Ca(2+) oscillations and waves by oscillating translocation and activation of protein kinase C. Curr. Biol. 11:1089–1097. http://dx.doi.org/10 .1016/S0960-9822(01)00326-8
- Daleke, D.L. 2003. Regulation of transbilayer plasma membrane phospholipid asymmetry. J. Lipid Res. 44:233–242. http://dx.doi.org/10.1194/jlr.R200019-JLR200
- Day, C.L., N.P. Seth, M. Lucas, H. Appel, L. Gauthier, G.M. Lauer, G.K. Robbins, Z.M. Szczepiorkowski, D.R. Casson, R.T. Chung, et al. 2003. Ex vivo analysis of human memory CD4 T cells specific for hepatitis C virus using MHC class II tetramers. J. Clin. Invest. 112:831–842.
- Deford-Watts, L.M., T.C. Tassin, A.M. Becker, J.J. Medeiros, J.P. Albanesi, P.E. Love, C. Wülfing, and N.S. van Oers. 2009. The cytoplasmic tail

- of the T cell receptor CD3 epsilon subunit contains a phospholipid-binding motif that regulates T cell functions. *J. Immunol.* 183:1055–1064. http://dx.doi.org/10.4049/jimmunol.0900404
- DeFord-Watts, L.M., D.S. Dougall, S. Belkaya, B.A. Johnson, J.L. Eitson, K.T. Roybal, B. Barylko, J.P. Albanesi, C. Wülfing, and N.S. van Oers. 2011. The CD3 zeta subunit contains a phosphoinositide-binding motif that is required for the stable accumulation of TCR-CD3 complex at the immunological synapse. *J. Immunol.* 186:6839–6847. http://dx.doi.org/10.4049/jimmunol.1002721
- Dustin, M.L., T. Starr, R. Varma, and V.K. Thomas. 2007. Supported planar bilayers for study of the immunological synapse. Curr Protoc Immunol. Chapter 18:Unit 18 13.
- Fairn, G.D., N.L. Schieber, N. Ariotti, S. Murphy, L. Kuerschner, R.I. Webb, S. Grinstein, and R.G. Parton. 2011. High-resolution mapping reveals topologically distinct cellular pools of phosphatidylserine. J. Cell Biol. 194:257–275. http://dx.doi.org/10.1083/jcb.201012028
- Folmer, D.E., R.P. Elferink, and C.C. Paulusma. 2009. P4 ATPases lipid flippases and their role in disease. *Biochim. Biophys. Acta.* 1791:628–635. http://dx.doi.org/10.1016/j.bbalip.2009.02.008
- Fridriksson, E.K., P.A. Shipkova, E.D. Sheets, D. Holowka, B. Baird, and F.W. McLafferty. 1999. Quantitative analysis of phospholipids in functionally important membrane domains from RBL-2H3 mast cells using tandem high-resolution mass spectrometry. *Biochemistry*. 38:8056–8063. http://dx.doi.org/10.1021/bi9828324
- Grakoui, A., S.K. Bromley, C. Sumen, M.M. Davis, A.S. Shaw, P.M. Allen, and M.L. Dustin. 1999. The immunological synapse: a molecular machine controlling T cell activation. *Science*. 285:221–227. http://dx.doi.org/10.1126/science.285.5425.221
- Hashimoto-Tane, A., T. Yokosuka, C. Ishihara, M. Sakuma, W. Kobayashi, and T. Saito. 2010. T-cell receptor microclusters critical for T-cell activation are formed independently of lipid raft clustering. *Mol. Cell. Biol.* 30:3421–3429. http://dx.doi.org/10.1128/MCB.00160-10
- Hirata, F., J. Axelrod, and F.T. Crews. 1979. Concanavalin A stimulates phospholipid methylation and phosphatidylserine decarboxylation in rat mast cells. *Proc. Natl. Acad. Sci. USA*. 76:4813–4816. http://dx.doi.org/10.1073/pnas.76.10.4813
- Huang, J., V.I. Zarnitsyna, B. Liu, L.J. Edwards, N. Jiang, B.D. Evavold, and C. Zhu. 2010. The kinetics of two-dimensional TCR and pMHC interactions determine T-cell responsiveness. *Nature*. 464:932–936. http://dx.doi.org/10.1038/nature08944
- Huppa, J.B., M. Axmann, M.A. Mörtelmaier, B.F. Lillemeier, E.W. Newell, M. Brameshuber, L.O. Klein, G.J. Schütz, and M.M. Davis. 2010. TCR-peptide-MHC interactions in situ show accelerated kinetics and increased affinity. *Nature*. 463:963–967. http://dx.doi.org/10.1038/nature08746
- Irvine, D.J., M.A. Purbhoo, M. Krogsgaard, and M.M. Davis. 2002. Direct observation of ligand recognition by T cells. *Nature*. 419:845–849. http://dx.doi.org/10.1038/nature01076
- Jordan, M.S., and G.A. Koretzky. 2010. Coordination of receptor signaling in multiple hematopoietic cell lineages by the adaptor protein SLP-76. Cold Spring Harb. Perspect. Biol. 2:a002501. http://dx.doi.org/10.1101/ cshperspect.a002501
- Kay, J.G., M. Koivusalo, X. Ma, T. Wohland, and S. Grinstein. 2012. Phosphatidylserine dynamics in cellular membranes. Mol. Biol. Cell. 23:2198–2212. http://dx.doi.org/10.1091/mbc.E11-11-0936
- Kuhns, M.S., M.M. Davis, and K.C. Garcia. 2006. Deconstructing the form and function of the TCR/CD3 complex. *Immunity*. 24:133–139. http://dx.doi.org/10.1016/j.immuni.2006.01.006
- Padilla-Parra, S., N. Audugé, H. Lalucque, J.C. Mevel, M. Coppey-Moisan, and M. Tramier. 2009. Quantitative comparison of different fluorescent protein couples for fast FRET-FLIM acquisition. *Biophys. J.* 97:2368–2376. http://dx.doi.org/10.1016/j.bpj.2009.07.044
- Reth, M. 1989. Antigen receptor tail clue. Nature. 338:383–384. http://dx.doi.org/10.1038/338383b0
- Samelson, L.E. 2002. Signal transduction mediated by the T cell antigen receptor: the role of adapter proteins. *Annu. Rev. Immunol.* 20:371–394. http://dx.doi.org/10.1146/annurev.immunol.20.092601.111357
- Schubert, D.A., S. Gordo, J.J. Sabatino Jr., S. Vardhana, E. Gagnon, D.K. Sethi, N.P. Seth, K. Choudhuri, H. Reijonen, G.T. Nepom, et al. 2012. Self-reactive human CD4 T cell clones form unusual immunological

- synapses. J. Exp. Med. 209:335–352. http://dx.doi.org/10.1084/jem.20111485
- Schuiki, I., and G. Daum. 2009. Phosphatidylserine decarboxylases, key enzymes of lipid metabolism. *IUBMB Life*. 61:151–162. http://dx.doi .org/10.1002/iub.159
- Shi, J., C.W. Heegaard, J.T. Rasmussen, and G.E. Gilbert. 2004. Lactadherin binds selectively to membranes containing phosphatidyl-L-serine and increased curvature. *Biochim. Biophys. Acta.* 1667:82–90. http://dx.doi .org/10.1016/j.bbamem.2004.09.006
- Sigalov, A.B., D.A. Aivazian, V.N. Uversky, and L.J. Stern. 2006. Lipid-binding activity of intrinsically unstructured cytoplasmic domains of multichain immune recognition receptor signaling subunits. *Biochemistry*. 45:15731–15739. http://dx.doi.org/10.1021/bi061108f
- Stauffer, T.P., S. Ahn, and T. Meyer. 1998. Receptor-induced transient reduction in plasma membrane PtdIns(4,5)P2 concentration monitored in living cells. Curr. Biol. 8:343–346. http://dx.doi.org/10.1016/S0960-9822(98)70135-6
- Sun, Y., R.D. Dandekar, Y.S. Mao, H.L. Yin, and C. Wülfing. 2011a. Phosphatidylinositol (4,5) bisphosphate controls T cell activation by regulating T cell rigidity and organization. *PLoS ONE*. 6:e27227. http://dx.doi.org/10.1371/journal.pone.0027227
- Sun, Y., R.N. Day, and A. Periasamy. 2011b. Investigating protein-protein interactions in living cells using fluorescence lifetime imaging microscopy. *Nat. Protoc.* 6:1324–1340. http://dx.doi.org/10.1038/nprot.2011.364
- Suzuki, J., M. Umeda, P.J. Sims, and S. Nagata. 2010. Calcium-dependent phospholipid scrambling by TMEM16F. *Nature*. 468:834–838. http:// dx.doi.org/10.1038/nature09583
- Valitutti, S., S. Müller, M. Cella, E. Padovan, and A. Lanzavecchia. 1995. Serial triggering of many T-cell receptors by a few peptide-MHC complexes. *Nature*. 375:148–151. http://dx.doi.org/10.1038/375148a0
- Vardhana, S., K. Choudhuri, R. Varma, and M.L. Dustin. 2010. Essential role of ubiquitin and TSG101 protein in formation and function of the central supramolecular activation cluster. *Immunity*. 32:531–540. http:// dx.doi.org/10.1016/j.immuni.2010.04.005
- Varma, R., G. Campi, T. Yokosuka, T. Saito, and M.L. Dustin. 2006. T cell receptor-proximal signals are sustained in peripheral microclusters and terminated in the central supramolecular activation cluster. *Immunity*. 25:117–127. http://dx.doi.org/10.1016/j.immuni.2006.04.010

- Wang, H., T.A. Kadlecek, B.B. Au-Yeung, H.E. Goodfellow, L.Y. Hsu, T.S. Freedman, and A. Weiss. 2010. ZAP-70: an essential kinase in T-cell signaling. Cold Spring Harb. Perspect. Biol. 2:a002279. http://dx.doi.org/10.1101/cshperspect.a002279
- Wucherpfennig, K.W., A. Sette, S. Southwood, C. Oseroff, M. Matsui, J.L. Strominger, and D.A. Hafler. 1994. Structural requirements for binding of an immunodominant myelin basic protein peptide to DR2 isotypes and for its recognition by human T cell clones. *J. Exp. Med.* 179:279–290. http://dx.doi.org/10.1084/jem.179.1.279
- Xu, C., E. Gagnon, M.E. Call, J.R. Schnell, C.D. Schwieters, C.V. Carman, J.J. Chou, and K.W. Wucherpfennig. 2008. Regulation of T cell receptor activation by dynamic membrane binding of the CD3epsilon cytoplasmic tyrosine-based motif. *Cell.* 135:702–713. http://dx.doi.org/10.1016/ j.cell.2008.09.044
- Yeung, T., M. Terebiznik, L. Yu, J. Silvius, W.M. Abidi, M. Philips, T. Levine, A. Kapus, and S. Grinstein. 2006. Receptor activation alters inner surface potential during phagocytosis. Science. 313:347–351. http://dx.doi.org/10.1126/science.1129551
- Yeung, T., G.E. Gilbert, J. Shi, J. Silvius, A. Kapus, and S. Grinstein. 2008. Membrane phosphatidylserine regulates surface charge and protein localization. *Science*. 319:210–213. http://dx.doi.org/10.1126/science .1152066
- Yeung, T., B. Heit, J.F. Dubuisson, G.D. Fairn, B. Chiu, R. Inman, A. Kapus, M. Swanson, and S. Grinstein. 2009. Contribution of phosphatidylserine to membrane surface charge and protein targeting during phagosome maturation. J. Cell Biol. 185:917–928. http://dx.doi.org/10.1083/jcb.200903020
- Yokosuka, T., and T. Saito. 2010. The immunological synapse, TCR microclusters, and T cell activation. Curr. Top. Microbiol. Immunol. 340:81–107. http://dx.doi.org/10.1007/978-3-642-03858-7_5
- Zhang, T.T., H. Li, S.M. Cheung, J.L. Costantini, S. Hou, M. Al-Alwan, and A.J. Marshall. 2009. Phosphoinositide 3-kinase-regulated adapters in lymphocyte activation. *Immunol. Rev.* 232:255–272. http://dx.doi.org/10.1111/j.1600-065X.2009.00838.x
- Zhang, H., S.P. Cordoba, O. Dushek, and P.A. van der Merwe. 2011. Basic residues in the T-cell receptor ζ cytoplasmic domain mediate membrane association and modulate signaling. *Proc. Natl. Acad. Sci. USA*. 108:19323–19328. http://dx.doi.org/10.1073/pnas.1108052108